16

Complementary Control of Intermittently Operating Renewable Sources with Short- and Long-Term Storage Plants

E. F. Fuchs and W. L. Fuchs
University of Colorado at Boulder, USA

1. Introduction

The deployment of renewable energy sources requires that neighborhood short- and long-term storage plants which complement the intermittent nature of their output, that is, produce electricity when the renewable plants are inactive and store electric energy when renewable plants generate more than the grid can accept. This chapter focuses on the interaction between conventional power plants with renewable sources and storage facilities. The various plants are modeled in the time domain and the resulting differential equation system is solved by available software. Results confirm that a complementary control permits the operation of renewable sources, paired with storage plants, within the frequency band of 59-61 Hz. The proper design of the time constants, choice of switching times/commands of storage plants, and the sufficient capability of the transmission lines (e.g., tie lines) are essential for steady-state and dynamic stability of a smart/micro grid as investigated in this chapter. Future research must concentrate on the measurement of the output powers of the various plants as a function of time and use these measurements for the timed switching commands.

1.1 Energy efficiency and reliability increases through interconnected power system

Prior to 1940 there were a limited number of interconnected power systems. Servicing loads was simple, as the systems were primarily radial circuits (Fig. 1a) and many power systems were operated in islanding mode. In more recent years interconnection of power systems has been favored (Fig. 1b), and within the US three power grids (Western, Eastern and Texan generation systems [ERCOT]) were established. Within these three power pools, many loop circuits with many load/generation buses and high levels of power exchange between neighboring companies exist. The latter point relates closely to interconnection advantages.

With no addition of actual generation capacity, it is possible to increase generation through interconnection. In the case of an outage of a generating unit, for example, power may be purchased from a neighboring company. The cost savings realized from lower installed capacity usually far outweigh the cost of the transmission circuits required to access neighboring companies. Fundamental and harmonic steady-state power flows are discussed in a recent book on power quality (E.F. Fuchs & Masoum, 2008a). Yet while energy

efficiency of an interconnected system is increased by more fully loading existing generation plants, efficiency decreases by transporting energy via transmission lines over larger distances. The average transmission loss within interconnected systems is about 8%.

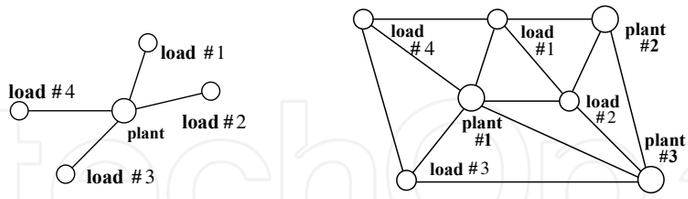

Figs. 1a,b. (a) Radial power system; (b) Interconnected power system

1.2 Future conventional and renewable energy sources

The generation mix (e.g., coal, natural gas, nuclear, hydro plants) of existing power systems will change in the future to mainly natural-gas fired plants, distributed renewable generation facilities (E. F. Fuchs & H. A. Fuchs, 2007) and storage plants. The ability to transition from the interconnected system to an islanding mode of operation must also be possible (E. F. Fuchs & F. S. Fuchs, 2008) to increase reliability. This means that any islanding system must have a frequency-leading plant ("frequency leader") in addition to renewable plants and storage plants. Renewable and storage plants cannot be frequency leaders because of their intermittent and limited output powers, respectively.

2. Review of current methods and issues of present-day frequency and voltage control

Present-day frequency/load and voltage control of interconnected systems takes place at the transmission level and is based on load-sharing and demand-side management. Load sharing relies on drooping characteristics (Wood, Wollenberg, 1984) (Fig. 2 and Figs. 4a, b, c) where natural gas, coal, nuclear and hydro plants or those with spinning reserves supply the additional load demand. If this additional load cannot be served by the interconnected plants, demand-side management (load shedding) will set in and some of the less important loads will be disconnected. This method of frequency/load control cannot

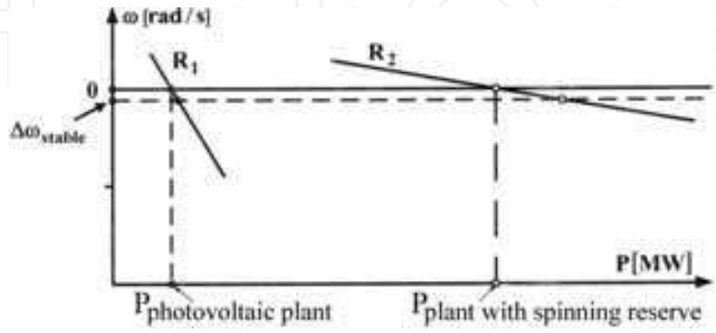

Fig. 2. Angular frequency versus output power: Stable frequency control relying on droop characteristics where a plant with spinning reserve operates continuously and a photovoltaic (PV) plant intermittently operates at its maximum output power due to peak-power tracking

be employed if renewable sources are operating at peak power in order to displace as much fuel as possible; it functions only as long as renewable energy represents a small fraction of overall generation capacity. As this fraction increases at either the distribution or transmission levels, frequency control problems will result. In today's interconnected systems, a frequency variation between f_{min}=59 Hz and f_{max}= 61 Hz, that is, $\Delta f = \pm$ 1.67% is acceptable (Fuller *et al.*, 1989). Voltage control is performed based on capacitor-bank switching, synchronous condensors and over/underexcitation of synchronous generators in power plants.

2.1 Isochronous control or frequency/load control of an isolated power plant with one generator only

Example #1: Fig. 3a illustrates the block diagram of governor, prime mover (steam turbine) and rotating mass (characterized by the momentum $M=\omega_o J$) and load of a turbo generator set [Wood & Wollenberg, 1984].

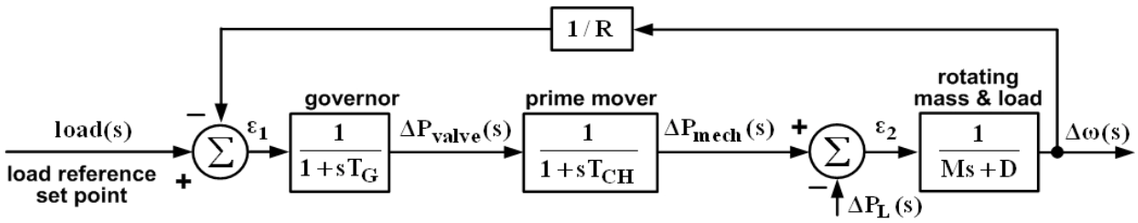

Fig. 3a. Block diagram of governor, prime mover and rotating mass & load at isochronous operation of power system, where D corresponds to the frequency-dependent load and $\Delta P_L(s)$ is the frequency-independent load

In Fig. 3a the parameters are as follows: Angular frequency change $\Delta\omega$ per change in generator output power ΔP, that is $R=\Delta\omega/\Delta P$=0.01 pu, the frequency-dependent load change ΔP_{L_freq} per angular frequency change $\Delta\omega$, that is $D=\Delta P_{L\_frequ}/\Delta\omega$=0.8 pu, step-load change $\Delta P_L(s)=\Delta P_L/s$=0.2/s pu, angular momentum of steam turbine and generator set M=4.5, base apparent power S_{base} =500 MVA, governor time constant T_G=0.01 s, valve changing/charging time constant T_{CH}=1.0 s, and load reference set point load(s)=1.0 pu.

a. Derive for Fig. 3a $\Delta\omega_{steady\ state}$ by applying the final value theorem. You may assume load reference set point load(s) = 1.0 pu, and $\Delta P_L(s)=\Delta P_L/s$=0.2/s pu. For the nominal frequency f*=60 Hz calculate the frequency f_{new} after the load change has taken place.
b. List the ordinary differential equations and the algebraic equations of the block diagram of Fig. 3a.
c. Use either Mathematica or Matlab to establish steady-state conditions by imposing a step function for load reference set point load(s) =1/s pu and run the program with a zero-step load change ΔP_L=0 (for 25 s) in order to establish the equilibrium condition without load step. After 25 s impose a positive step-load change of $\Delta P_L(s)=\Delta P_L/s$=0.2/s pu to find the transient response of $\Delta\omega(t)$ for a total of 50 s, and at 50 s impose a negative step-load change of $\Delta P_L(s)=\Delta P_L/s$= - 0.2/s pu to find the transient response of $\Delta\omega(t)$ for a total of 75 s.

The solution to this example is given in Application Example 12.7 of (E.F. Fuchs & Masoum, 2011) and illustrated in Fig. 3b.

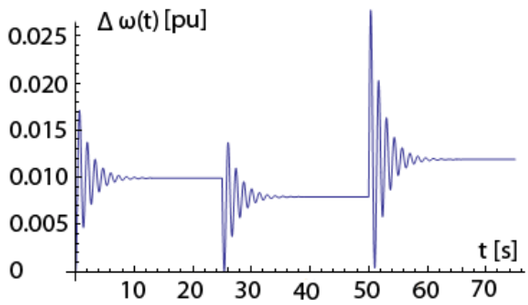

Fig. 3b. Angular frequency change Δω(t) for a positive load-step at time t=25 s and a negative load step at time t=50 s

2.2 Load/frequency control with droop characteristics of an interconnected power system broken into two areas each having one generator

Example #2: Fig. 4a shows the block diagram of two generators interconnected by a transmission tie line (Wood & Wollenberg, 1984).

Data for generation set (steam turbine and generator) #1: Angular frequency change $\Delta\omega_1$ per change in generator output power ΔP_1, that is $R_1=\Delta\omega_1/\Delta P_1=0.01$ pu (e.g., coal-fired plant), the frequency-dependent load change ΔP_{L1_frequ} per angular frequency change $\Delta\omega_1$, that is $D_1=\Delta P_{L1\_frequ}/\Delta\omega_1=0.8$ pu, positive step-load change $\Delta P_{L1}(s)=\Delta P_{L1}/s=0.2/s$ pu, angular momentum of steam turbine and generator set $M_1=4.5$, base apparent power $S_{base}=500$ MVA, governor time constant $T_{G1}=0.01$ s, valve changing/charging time constant $T_{CH1}=0.5$ s, and load $ref_1(s)=0.8$ pu.

Data for generation set (steam turbine and generator) #2: Angular frequency change $\Delta\omega_2$ per change in generator output power ΔP_2, that is $R_2=\Delta\omega_2/\Delta P_2=0.02$ pu (e.g., coal-fired plant), the frequency-dependent load change ΔP_{L2_frequ} per angular frequency change $\Delta\omega_2$, that is $D_2=\Delta P_{L2\_frequ}/\Delta\omega_2=1.0$ pu, negative step-load change $\Delta P_{L2}(s)=\Delta P_{L2}/s=-0.2/s$ pu, angular momentum of steam turbine and generator set $M_2=6$, base apparent power $S_{base}=500$ MVA, governor time constant $T_{G2}=0.02$ s, valve changing/charging time constant $T_{CH2}=0.75$ s, and load $ref_2(s)=0.8$ pu.

Data for tie line: $T=377/X_{tie}$ with $X_{tie}=0.2$ pu.

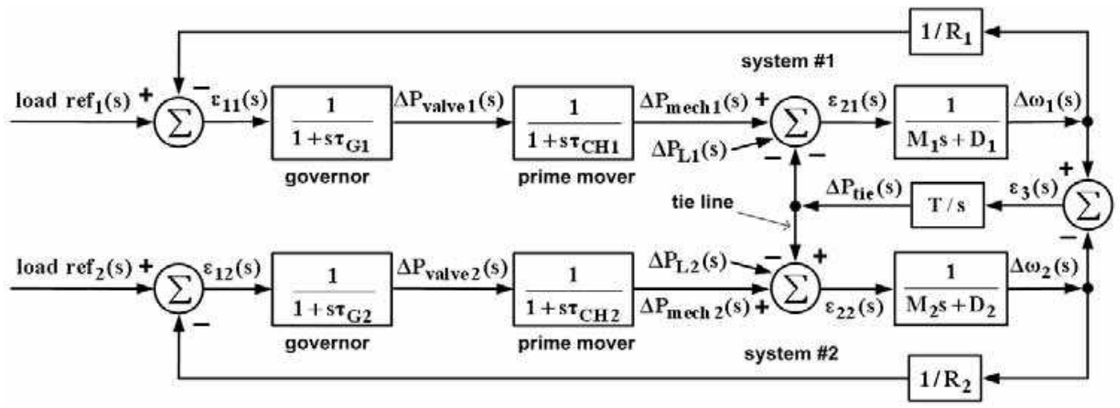

Fig. 4a. Block diagram of two interconnected generators through a tie (transmission) line, where D_1 and D_2 correspond to the frequency-dependent loads and $\Delta P_{L1}(s)$ and $\Delta P_{L2}(s)$ are the frequency-independent loads

a. List the ordinary differential equations and the algebraic equations of the block diagram of Fig. 4a.
b. Use either Mathematica or Matlab to establish steady-state conditions by imposing a step function for load $ref_1(s)=0.8/s$ pu, load $ref_2(s)=0.8/s$ pu and run the program with zero step-load changes $\Delta P_{L1}=0$, $\Delta P_{L2}=0$ (for 10 s) in order to establish the equilibrium condition. After 10 s impose positive step-load change $\Delta P_{L1}(s)=\Delta P_{L1}/s=0.2/s$ pu, and after 30 s impose negative step-load change $\Delta P_{L2}(s)=\Delta P_{L2}/s= - 0.2/s$ pu to find the transient response $\Delta\omega_1(t)=\Delta\omega_2(t)=\Delta\omega(t)$ for a total of 50 s. Repeat part b) for $R_1=0.5$ pu, (e.g., wind-power plant), and $R_2= 0.01$ pu (e.g., coal-fired plant).

The solution to this example is given in Application Example 12.8 of (E.F. Fuchs & Masoum, 2011) and illustrated in Figs. 4b,c.

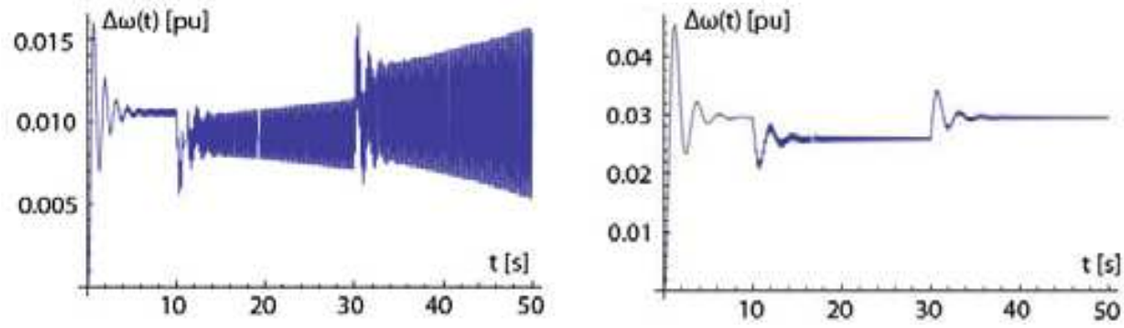

(b) (c)

Figs. 4b,c. (b) Angular frequency change $\Delta\omega(t)$ for unstable operation due to the approximately same droop characteristics ($R_1=0.01$ pu) and ($R_2=0.02$ pu); (c) Angular frequency change $\Delta\omega(t)$ for stable operation due to the different droop characteristics ($R_1=0.5$ pu) and ($R_2=0.01$ pu)

3. Intermittently operating renewable plants

Portfolio standards will drive significant increases in renewable energy resources. Photovoltaic (PV) is expected to increase dramatically, with power penetration levels of 10-50% occurring in local areas within the next decade (Defree, 2009). Regions with large PV plants and relatively soft grids, such as the 8 MW SunEdison plant in Colorado's San Luis valley (on Xcel's Energy's grid) have experienced power quality issues primarily related to current harmonics at low PV output levels. Such PV systems can also experience rapidly fluctuating outputs. Fig. 5 (National Renewable Energy Laboratory [NREL], 2009) illustrates solar radiation levels on a horizontal plate during one recent 24-hour period. As can be seen from this time series (1-minute sampling rate) data, rapid transients occur within minutes. For the date shown, 67 transients occurred where radiation levels changed by more than 30% of the peak radiation level within one minute. These radiation transients directly affect PV output and place additional demands on spinning reserves. Control of renewable sources occurs at the distribution level and communication between transmission and distribution levels becomes important. A new frequency-control algorithm must therefore be designed to replace some of the large conventional plants (e.g., coal, nuclear, natural gas) by a great number of much smaller renewable and storage plants. While PV revenue growth slowed slightly in the last year, Gartner Group projects that PV implementation, measured on a power basis, will grow to 23.4 GW by 2013 (Defree, 2009) due both to consumer demand and portfolio standards requiring more renewable energy generation.

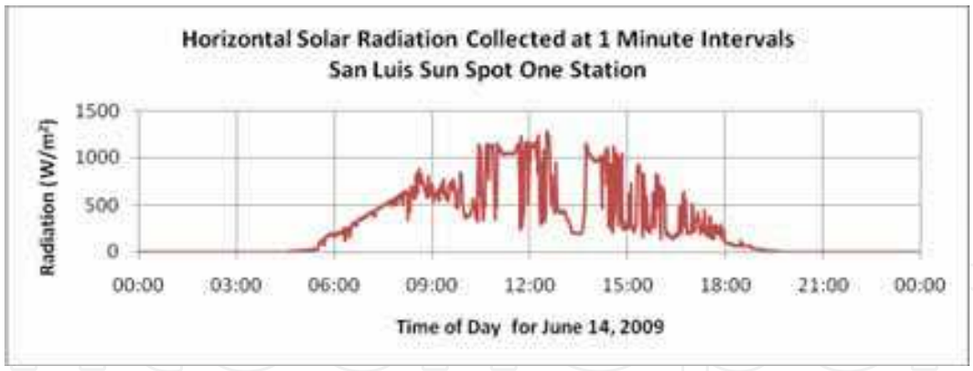

Fig. 5. Horizontal plate solar radiation in San Louis Valley, (NREL, 2009)

Similarly, high windpower (WP) penetrations have already occurred in Europe, and are likely to occur in regions of the US during the next decade. Areas relying on WP today are also experiencing power quality and control problems. PV systems experience different--typically faster--transients than wind systems because they are normally interconnected with inverters rather than rotating machines, which have virtually no inertia and low ride-through capacities. Residential-scale single-phase inverters are typically not designed to generate reactive power and are operated at unity power factor. A supply of reactive power to the grid would entail an increased DC voltage at the inverter input, as will be discussed in a later section. To date, most WP has been deployed in relatively large units from 1-5 MW dispersed turbines connected at the distribution level to hundreds of MW in wind farms connected at the transmission level. PV is frequently deployed in small units interspersed with residential or commercial loads in larger plants connected at the transmission level.

3.1 Design of PV plants

Fig. 6 illustrates the insolation within the contiguous United States in terms of kWh/m² per day. In Boulder, Colorado, one can expect (5.5-6.0) kWh/m² per day.

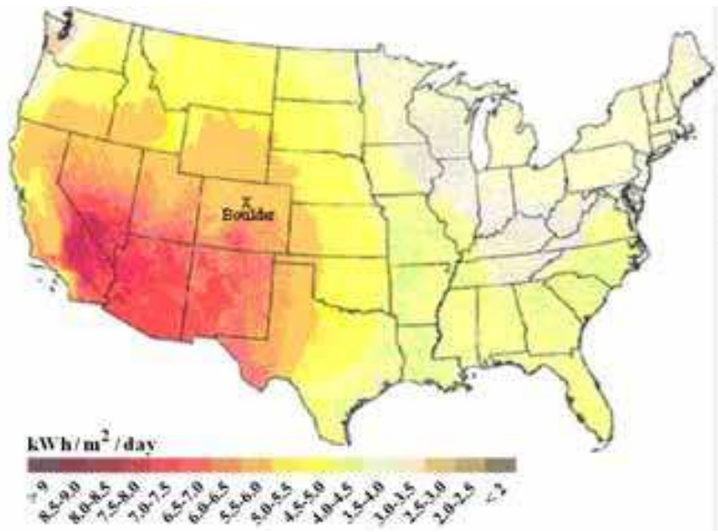

Fig. 6. Insolation or irradiance levels within the United States (created and prepared by NREL, 2008 for the U.S. Department of Energy)

The PV system of Fig. 7a installed and put on line in September 2007 generated during a recent 14-month period the data of Table 1 indicating the cumulative net meter reading $E_{net\ meter}$, the total generated AC energy $E_{generated}$, the AC energy supplied to the utility Xcel $E_{supplied\ Xcel}$, the AC energy consumed by the residence $E_{residence}$, and the CO_2 emissions avoided. The connection cost charged by the utility $C_{connection}$ is \$8.55 per month. Fig. 7b illustrates the circuit components required for net metering.

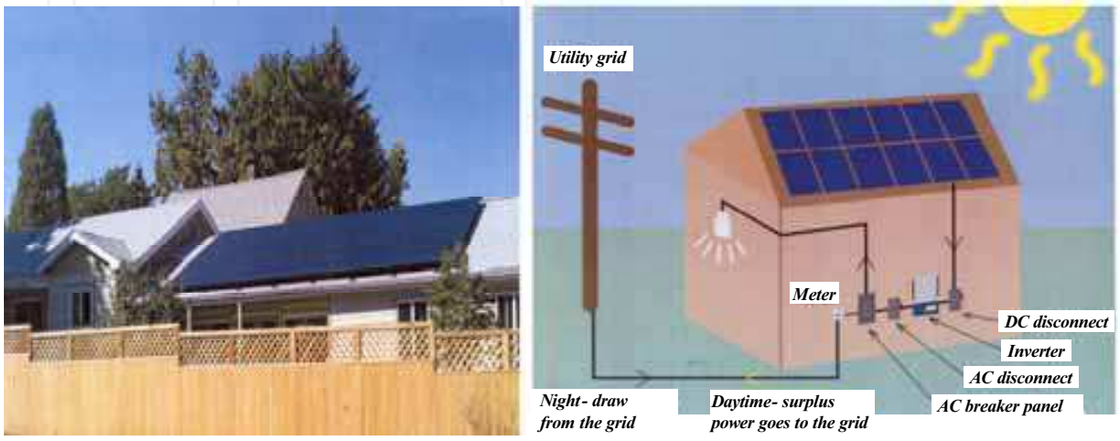

(a) (b)

Figs. 7a,b. (a) Residence with solar panels in Boulder, CO, 2007; (b) Net metering (Courtesy of Namasté Solar, 4571 North Broadway, Boulder, CO 80304), 2007

time period (readings recorded at end of each time period)	cumulative net meter reading $E_{net\ meter}$ [kWh]	cumulative total kWh generated $E_{generated}$ [kWh]	excess energy to Xcel $E_{supplied\ Xcel}$ [kWh]	energy consumed by residence $E_{residence}$ [kWh]	CO_2 emission avoided [lbs-force]
1/1/10-1/31/10	90,131	18,846	75	401	32,037
2/1/10-2/28/10	90,104	19,276	27	403	32,770
3/1/10-3/31/10	89,674	19,931	430	225	33,882
4/1/10-4/30/10	89,078	20,724	596	197	35,230
5/1/10-5/31/10	88,354	21,644	724	196	36,795
6/1/10-6/30/10	87,652	22,512	702	166	38,271
7/1/10-7/31/10	87,020	23,395	632	251	39,772
8/1/10-8/31/10	86,330	24,288	690	203	41,290
9/1/10-10/2/10	85,661	25,143	669	186	42,742
10/3/10-10/31/10	85,314	25,681	347	191	43,658
11/1/10-11/30/10	85,075	26,175	239	255	44,498
12/1/10-12/31/10	84,934	26,575	141	259	45,177
1/1/10-1/31/10	84,793	27,009	141	293	45,916
2/1/10-2/28/10	84,558	27,461	235	217	46,684

Table 1. Generated data of PV plant of Fig. 7a during a recent 14-month timeframe

Figs. 1.4, 1.5, and 1.6 of reference (E.F. Fuchs & Masoum, 2011) show the energy production of the 6.15 kW_{DC} plant of Fig. 7a during the entire year 2009, during October 2009, and

during the 31st of October 2009, respectively. As can be seen from Fig. 1.5, since weather conditions make it likely there will be little energy production during periods of two to three days at a time, energy storage becomes important. The design data and the payback period information of the 6.15 kW_{DC} PV system of Fig. 7a are given in (E.F. Fuchs & Masoum, 2011).

Example #3: Design of a P_{AC}=5.61 kW PV power plant for a residence

A PV power plant consists of solar array, peak (maximum)-power tracker (Masoum *et al.*, 2002; Masoum *et al.*, 2004a), a step-up/step-down DC-to-DC converter, a deep-cycle battery for part f) only, a single-phase inverter, single-phase transformer, and residence which requires a maximum inverter AC output power of P_{inv}^{max}=5.61 kW as shown in Fig. 8. Note the maximum inverter output AC power has been specified because the entire power must pass through the inverter for all operating modes as explained below. In addition, inverters cannot be overloaded even for a short time due to the low heat capacity of the semiconductor switches. The modulation index of inverter is m=0.5 in order to guarantee a sinusoidal output current of the inverter neglecting pulse-width-modulated (PWM) switching harmonics.

Three operating modes will be investigated: In part f) the *operating mode #1* is a stand-alone configuration (700 kWh are consumed per month). In part g) the *operating mode #2* is a configuration where the entire energy (700 kWh) is consumed by the residence and the utility system is used as storage device only. In part h) the *operating mode #3* is a configuration where 300 kWh are consumed by the residence and 400 kWh are sold to the utility.

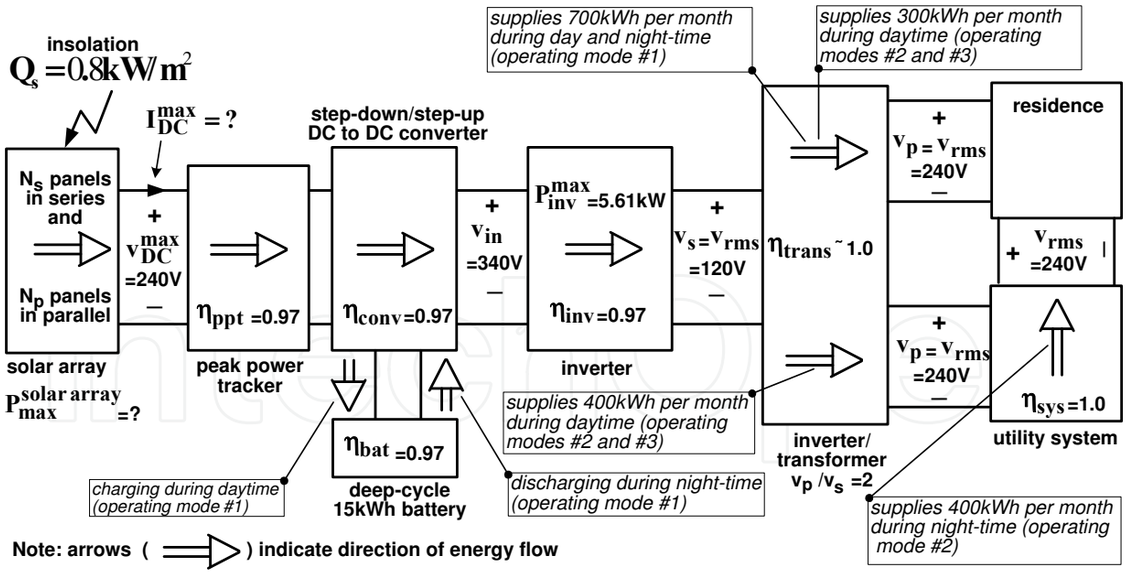

Fig. 8. Block diagram of a PV plant power plant for a residence

a. The power efficiencies of the maximum power tracker, the step-up/step-down DC-to-DC converter, the battery, and the inverter are 97 % each, while that of the transformer is about 1.00. What maximum power $P_{max}^{solar\ array}$ must be generated by the solar array, provided during daytime E_{month_day}=300 kWh will be delivered via the inverter to the

residence (without storing this energy in battery), and sufficient energy will be stored in the battery so that the battery energy of E_{month_night}=400 kWh can be delivered during nighttime by the battery via the inverter to the residence: that is, a total of E_{month}= E_{month_day} + E_{month_night} =700 kWh can be delivered to the residence during one month?

b. For a commercially available solar panel the V-I characteristic of Fig. 9a was measured at an insolation of Q_s=0.8 kW/m². Plot the power curve of this solar panel: $P_{panel}=f(I_{panel})$.

c. At which point of the power curve $P_{panel}=f(I_{panel})$ would one operate assuming Q_s=0.8 kW/m² is constant? What values for power, voltage and current correspond to this point?

d. How many solar panels would one have to connect in series (N_s) in order to achieve a DC output voltage of $V_{DC}^{max} = 240$ V of the solar array? How many solar panels would one have to connect in parallel (N_p) in order to generate the inverter output power P_{inv}^{max} =5.61 kW?

e. How much would be the purchase price of this solar power plant, if 1 kW installed output capacity of the inverter (this includes the purchase and installation costs of solar cells + peak-power tracker + DC-to-DC converter + inverter) costs $3,000 (after utility rebates and state/federal government tax-related subsidies)? Without tax rebates and subsidies the buyer would have to pay about $5,000 per 1 kW installed output power capacity.

f. *Operating mode #1:* What is the payback period (in years, without taking into account interest payments) of this solar plant if the residence uses 700 kWh per month at an avoided cost of $0.20/kWh (includes service fees and tax)? One may assume that this solar plant can generate every month 700 kWh and there is no need to buy electricity from the utility: 300 kWh per month will be used in the residence during daytime and during nighttime 400 kWh per month will be supplied via inverter from the battery to the residence. However, there is a need for the use of a 30 kWh deep-cycle battery as a storage element so that electricity will be available during hours after sunset. This battery must be replaced every four years at a cost of $3,000.

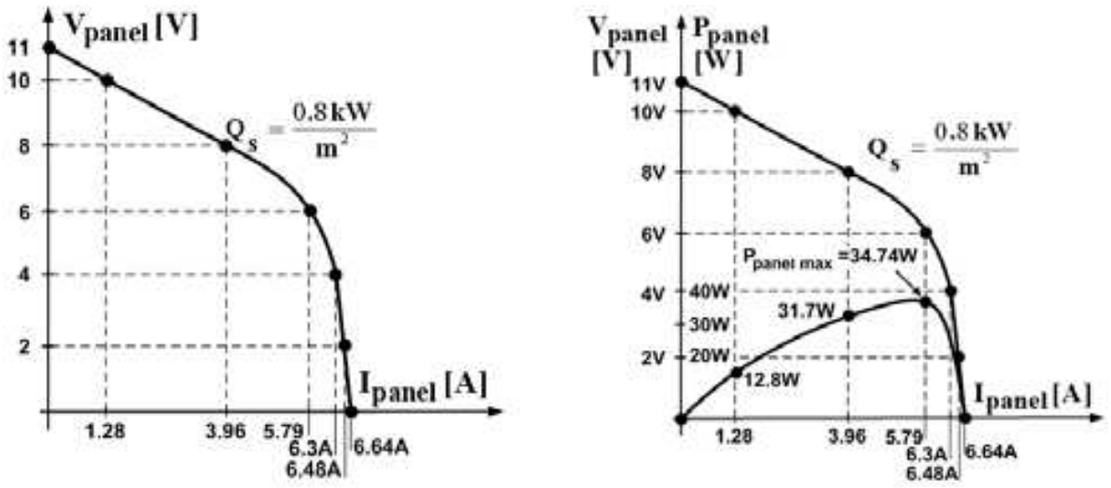

(a) (b)

Figs. 9a,b. (a) V-I characteristic of one solar panel; (b) P-I characteristic of one solar panel

g. *Operating mode #2:* What is the payback period (in years, without taking into account interest payments) of this solar plant if the residence uses 300 kWh per month at an avoided cost of $0.20 per kWh? One may assume that this solar plant can generate 700 kWh per month and feeds 400 kWh into the power system of the utility company, which reimburses the plant owner $0.20 per kWh (so-called "net metering"), in which case there is no need for a battery as a storage element because electricity can be supplied by the utility after sunset: 400 kWh at $0.20 per kWh. There is a connection charge of $8.55 per month.

h. *Operating mode #3:* What is the payback period (in years, without taking into account interest payments) of this solar plant if the residence uses 300 kWh per month at an avoided cost of $0.20 per kWh? One may assume that this solar plant can generate every month 700 kWh of which every month the solar plant feeds 400 kWh into the power system of the utility company which reimburses the plant owner $0.06 per kWh. There is a connection charge of $8.55 per month.

i. Which power plant configuration (f, g or h) is more cost effective (e.g., has the shortest payback period)?

j. What is the total surface of the solar panels provided the efficiency of solar cells is 15% at Q_s=0.8 kW/m²?

k. Instead of obtaining tax rebates and state/federal government subsidies the owner of a PV power plant obtains a higher price (feed-in tariff) for the electricity delivered to the utility: provided 700 kWh are fed into the utility grid at a reimbursement cost of $0.75/kWh and the utility supplies 300 kWh to the residence at a cost of $0.20/kWh, what is the payback period if the entire plant generating 5.61 kW_{AC} (there are no batteries required for storage) costs $30,000? One may neglect interest payments, and there is a connection charge of $8.55 per month.

l. Repeat part k) taking into account interest payments of 4.85%.

Solution:

a. The required maximum power output of the solar array is

$$P_{max}^{\text{solar array}} = \frac{\frac{300\text{kWh}}{700\text{kWh}} \cdot P_{inv}^{max}}{\eta_{ppt} \cdot \eta_{con} \cdot \eta_{inv}} + \frac{\frac{400\text{kWh}}{700\text{kWh}} \cdot P_{inv}^{max}}{\eta_{ppt} \cdot (\eta_{con})^2 \cdot (\eta_{bat})^2 \eta_{inv}}, \quad (1)$$

whereby the first term is the power consumed by the residence during daytime, and the second term corresponds to the energy stored in the battery during daytime and consumed by the residence during nighttime (delivered by battery).

$$P_{max}^{\text{solar array}} = \frac{\frac{300\text{kWh}}{700\text{kWh}} \cdot 5.61}{(0.97)^3} + \frac{\frac{400\text{kWh}}{700\text{kWh}} \cdot 5.61}{(0.97)^6} = 2.634\text{ kW} + 3.848\text{ kW} = 6.483\text{ kW}. \quad (2)$$

b. Fig. 9b illustrates the P-I characteristic of one solar panel.

c. Operation at the knee of the V_{panel}-I_{panel} characteristic yields the voltage $V_{panel}^{max} = 6\text{V}$ and the current $I_{panel}^{max} = 5.79\text{A}$ resulting in the peak or maximum (Masoum *et al.*, 2002, and Masoum *et al.*, 2004a) power $P_{panel}^{max} = 34.74\text{W}$.

d. The number of in series connected panels is $N_s = V_{DC}^{max} / V_{panel}^{max} = 240/6 = 40$. The DC current delivered by the solar array is $I_{DC} = P_{max}^{solar\ array} / V_{DC}^{max} = 6483/240 = 27.01$ A. From this follows the number of panels in parallel $N_p = I_{DC} / I_{panel}^{max} = 27.01/5.79 = 4.66$. To be on the safe side one chooses $N_{p\_modified}=5$ panels in parallel. The choice of 5 panels in parallel increases the available maximum solar array output power to $P_{max\ modified}^{solar\ array} = (5/4.66) \cdot 6.483\text{kW} = 6.956\text{kW}$ and the inverter output power must be increased as well $P_{inv}^{max\ modified} = (5/4.66) \cdot 5.61\text{kW} = 6.02\text{kW}$.
e. Purchase cost of solar power plant (modified version, without battery) cost=($3000/kW) · 6.02kW =$18,058.
f. Payback period if battery is used as storage device: Avoided payments to utility per year are $700\text{kWh} \cdot 12 \cdot \$0.20/\text{kWh} = \$1680$ resulting in the cost-benefit relation $1680(years)= $18058+($3000/4)(years) or $(years)_f$ =19.42.
g. Payback period if utility system is used a storage device and a connection charge to the utility ($8.55) is taken into account resulting in $1680(years) = $18058+$8.55 · 12(years) or $(years)_g$=11.45.
h. Payback period if 400 kWh per month are sold to utility: Avoided payments to utility are 300 kWh ·12·$0.20/kWh=$720 per year resulting in the cost-benefit relation $720 (years) + (400kWh·12·$0.06/kWh)(years)=$18,058+$8.55·12(years) or $(years)_h$=19.95.
i. Configuration with utility as storage device (case g) has the shortest payback period.
j. The required solar array area is area= $P_{max\ modified}^{solar\ array} / Q_s \cdot \eta_{cell} = \frac{6.956\text{kW}}{0.8 \cdot 0.15} = 58\text{m}^2$.
k. The income is $(700\text{kWh} \cdot \$0.75/\text{kWh}) \cdot 12(\text{years}) = \$6300(\text{years})$ or payback period based on income=expenses is $6,300(years)=$30,000+$300 ·12 · 0.2 (years)+$8.55·12 (years) or $(years)_k$ =5.48.
l. Same as k) but with interest payments results in the cost-benefit relation (6,300-720-102.6)· (years)=30,000(1.0485)$^{(years)}$. No payback period exists.

3.2 Components of short-term and long-term storage and renewable energy plants

Electric storage components can store electricity in DC form only. For this reason AC-to-DC converters (rectifiers), DC–to-AC converters (inverters), and DC-to-DC converters (step-down and step-up) must be relied on. All types of converters are discussed in (E.F. Fuchs & Masoum, 2011).

3.2.1 The role and design of short-term and long-term storage plants

Short-term storage devices such as batteries, fuel cells, supercapacitors and flywheels can be put online within a few 60 Hz cycles, but cannot provide energy for more than about 10 minutes; flow batteries and variable-speed hydro plants, however, can change their load within a few 60 Hz cycles and are able to deliver power for days. Long-term storage plants such as constant-speed (pump)-hydro storage and compressed air plants require a start-up time of about 6-10 minutes, but can operate for several hours or even days. Two short-term storage plants will be analyzed in a later section.

3.2.2 Pulse-width-modulated (PWM) rectifier

Rectifiers (i.e., Fig. 10) are an integral part for the conversion of AC to DC of most intermittently operating renewable sources such as PV plants, WP plants and storage plants. Fig. 10 shows one type of rectifier which is used within a three-phase power system. This rectifier is analyzed with PSpice where the input and output voltage relations can be determined as a function of the duty cycle (E.F. Fuchs & Masoum, 2011).

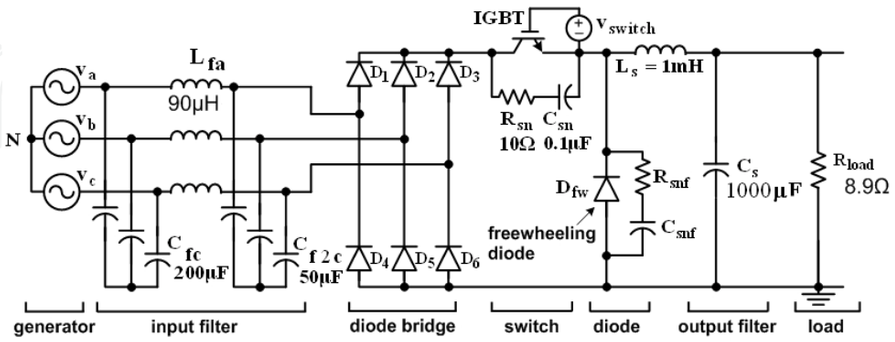

Fig. 10. Controlled three-phase rectifier with self-commutated switch

*Three-phase rectifier input voltages	*switch
Va 1 0 sin(0 465 60 0 0 0)	MOS 9 15 12 12 SMM
Vb 2 0 sin(0 465 60 0 0 -120)	*snubber resistors and capacitors
Vc 3 0 sin(0 465 60 0 0 -240)	Rsn 9 11 10
*switch gating signal of 3kHz	Csn 11 12 0.1u
vg 15 12 pulse(0 50 10u 0n 0n 166.6u	Rsnf 12 13 10
333u)	Csnf 13 10 0.1u
*diodes	*output filter and load resistor
D1 5 9 ideal	Ls 12 14 0.001
D2 10 7 ideal	Cs 14 10 1000u
D3 6 9 ideal	Rload 14 10 8.9
D4 10 5 ideal	*Model for MOSFET
D5 7 9 ideal	.model SMM NMOS(level=3 gamma=0
D6 10 6 ideal	kappa=0 tox=100n rs=0 kp=20.87u l=2u w=2.9
Dfw 10 12 ideal	+ delta=0 eta=0 theta=0 vmax=0 xj=0 uo=600
*input filter	phi=0.6 vto=0 rd=0 cbd=200n pb=0.8
Lfa 1 5 90u	+ mj=0.5 cgso=3.5n cgdo=100p rg=0 is=10f)
Lfb 2 6 90u	*diode model
Lfc 3 7 90u	.model ideal d(is=1p)
Cfa 1 4 200u	*options for improvement of convergence
Cfb 2 4 200u	.options abstol=10u chgtol=10p reltol=0.1
Cfc 3 4 200u	vntol=100m itl4=200 itl5=0
Rf1 4 10 10meg	.tran 0.5u 350m 300m 0.5m
Cf2a 5 8 50u	*plotting software
Cf2b 6 8 50u	.probe
Cf2c 7 8 50u	*fourier analysis
Rf2 8 10 10meg	.four 60 60 I(Rload)
	.end

Table 2. PSpice input program for PWM rectifier operation

The PSpice program is listed in Table 2 and the computed results are given in Table 3. Figs. 11a, b illustrate some of the results of Table 3. For a duty cycle of 0.05, a very high AC input voltage is required while at a duty cycle of 0.95 the AC input voltage is very low. In practice the duty cycle may vary between 25 and 75%. For very high power ranges thyristors or gate-turn-off (GTO) thyristors may be more suitable as discussed in Chapter 5 of (E.F. Fuchs & Masoum, 2011).

δ=0.05	$I_{DC\ load}$=45.05A	$V_{DC\ load}$=400.95 V	$V_{AN\ max}$=3000 V
δ=0.25	$I_{DC\ load}$=45.29A	$V_{DC\ load}$=403.08 V	$V_{AN\ max}$=890 V
δ=0.50	$I_{DC\ load}$=45.22A	$V_{DC\ load}$=402.46 V	$V_{AN\ max}$=465 V
δ=0.75	$I_{DC\ load}$=45.40A	$V_{DC\ load}$=404.06 V	$V_{AN\ max}$=320 V
δ=0.95	$I_{DC\ load}$=45.16A	$V_{DC\ load}$=401.92 V	$V_{AN\ max}$=256 V

Table 3. Dependency of the input voltage $V_{AN\ max}$ of a three-phase rectifier for given output voltages and currents, $V_{DC\ load}$, and $I_{DC\ load}$, respectively, at given duty cycles δ of the self-commutated switch (insulated gate bipolar transistor, IGBT).

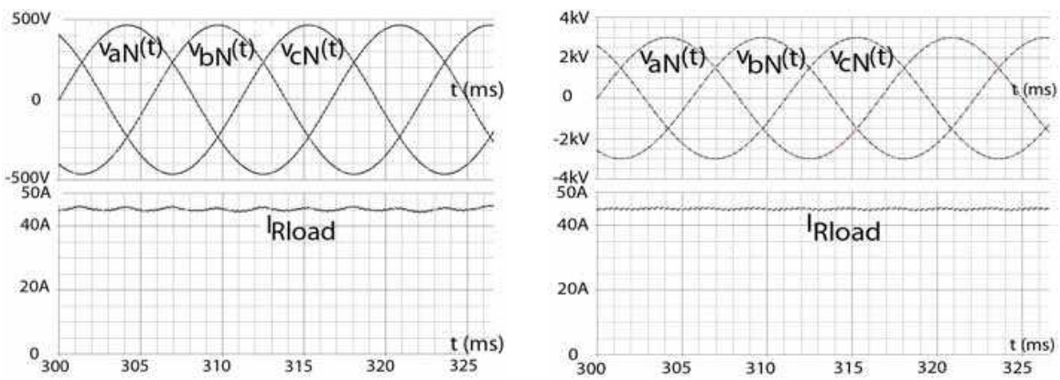

(a) (b)

Figs. 11a,b. Rectifier input AC voltages and output DC current: (a) For a duty cycle of δ=50%; (b) For a duty cycle of δ=5% (see Table 3)

3.2.3 Current-controlled, PWM voltage–source inverter

Similar to rectifiers, inverters (see for example Figs. 12a, b) must be employed for some of the renewable energy sources and for storage plants to convert DC to AC.

Table 4 lists the PSpice program on which the results of Table 5 are based. This latter table illustrates the dependency of the input DC voltage V_{DC} of inverter as a function of the output power factor angle Φ, that is, the angle between phase current of inverter $I_{rms\ ph}$ and line-to-neutral voltage $V_{rms\ l\text{-}n}$ of power system as well as the modulation index m (E.F. Fuchs & Masoum, 2008a). Figs. 13a, b illustrate some of the results of Table 5. According to (IEEE Standard 519, 1992; IEC 61000-3-2, 2001-10; E.F. Fuchs & Masoum, 2008a) a total harmonic distortion of the inverter output current I_{THDi} of about 3% --ignoring the switching ripple which can be mitigated by an output filter as indicated in Fig. 12a-- is acceptable. By decreasing the modulation index m, say m=0.5, which requires an increased V_{DC}, and by increasing the wave shaping inductance L_w an almost ideal sinusoid for the output current can be achieved and reactive power can be supplied to the power system.

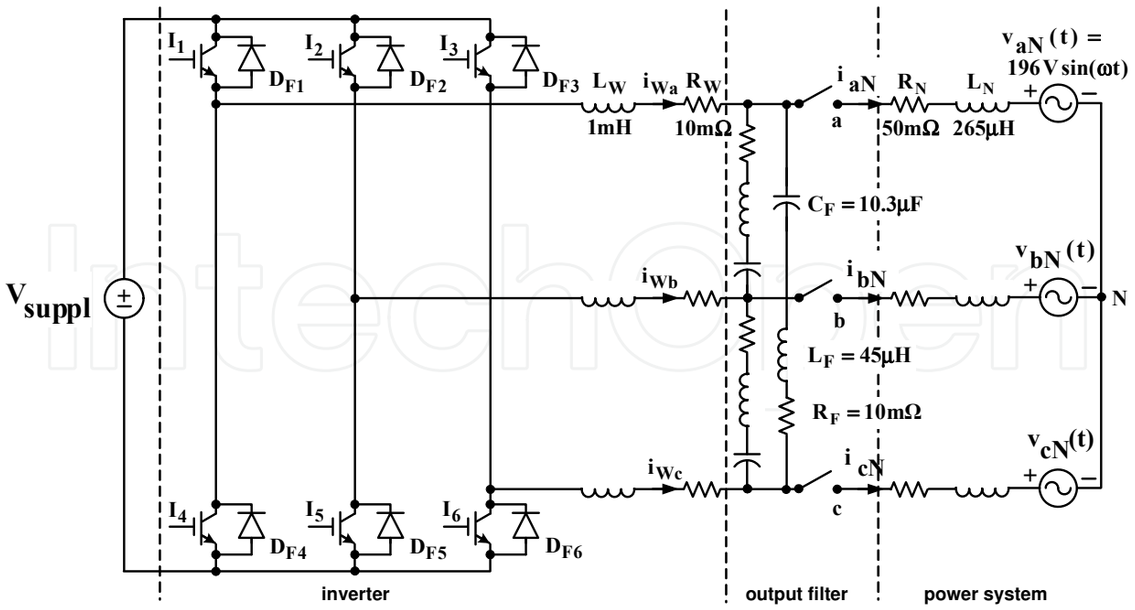

Fig. 12a. Current-controlled, PWM voltage-source inverter feeding power into utility system

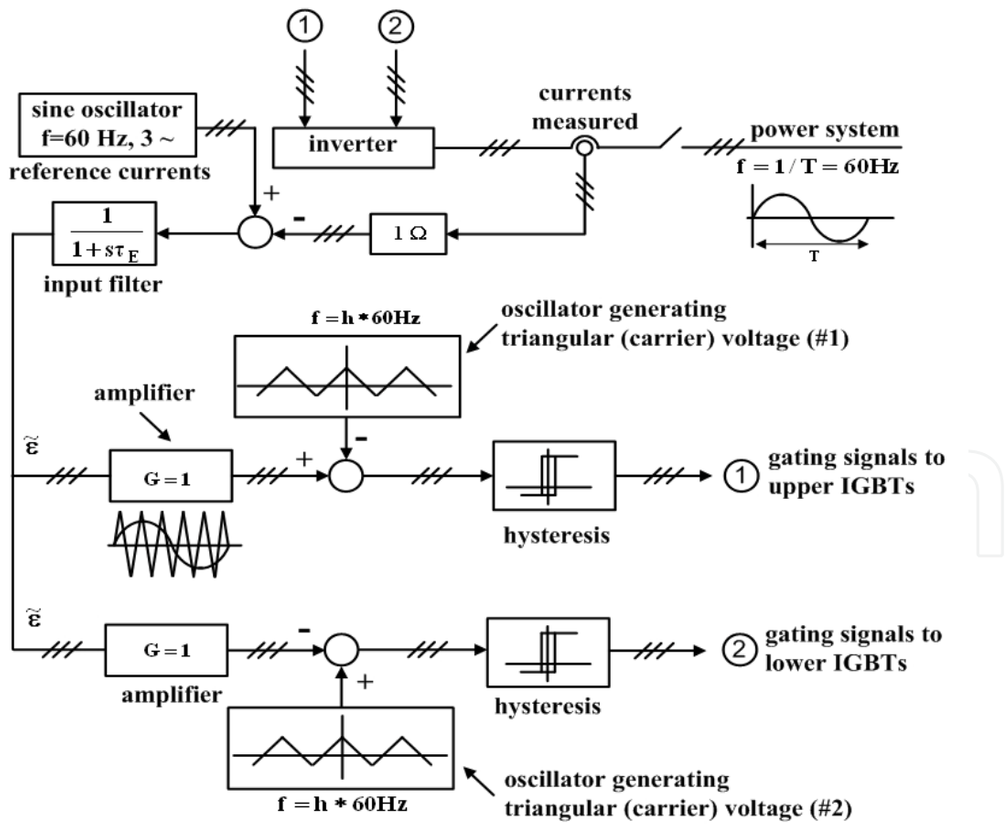

Fig. 12b. Block diagram of control circuit for current-controlled, PWM voltage–source inverter based on P-control

```
*Current-controlled pulse-width-
modulated (PWM) voltage-source
inverter
vsuppl 2 0 360
*switches
msw1 2 11 10 10 qfet
dsw1 10 2 diode
msw5 2 21 20 20 qfet
dsw5 20 2 diode
msw3 2 31 30 30 qfet
dsw3 30 2 diode
msw4 10 41 0 0 qfet
dsw4 0 10 diode
msw2 20 51 0 0 qfet
dsw2 0 20 diode
msw6 30 61 0 0 qfet
dsw6 0 30 diode
*waveshaping inductors
L_w1 10 15 1m
L_w2 20 25 1m
L_w3 30 35 1m
R_w1 15 16 10m
R_w2 25 26 10m
R_w3 35 36 10m
*current references in terms of voltages
vref1 12 0 sin(0 56.6 60 0 0 0)
vref2 22 0 sin(0 56.6 60 0 0 -120)
vref3 32 0 sin(0 56.6 60 0 0 -240)
eout1 13 0 15 16 100
eout2 23 0 25 26 100
eout3 33 0 35 36 100
*errorsignals produced as difference
between vr and eout
rdiff1 12 13a 1k
rdiff2 22 23a 1k
rdiff3 32 33a 1k
cdiff1 12 13a 1u
cdiff2 22 23a 1u
cdiff3 32 33a 1u
rdiff4 13a 13 1k
rdiff5 23a 23 1k
rdiff6 33a 33 1k
ecin1 14 0 12 13a 2
ecin2 24 0 22 23a 2
ecin3 34 0 32 33a 2
*Lfi1 16 15b 45u
*Lfi2 26 25b 45u
*Lfi3 36 35b 45u
*rfi1 15b 15c 0.01
*rfi2 25b 25c 0.01
*rfi3 35b 35c 0.01
*cfi1 15c 26 10.3u
*cfi2 25c 36 10.3u
*cfi3 35c 16 10.3u
*parameters of power system with a line-to-
line voltage of 340 V (amplitude)
RM1 16 18 50m
LM1 18 19 265u
Vout1 19 123 sin(0 196 60 0 0 -30)
RM2 26 28 50m
LM2 28 29 265u
Vout2 29 123 sin(0 196 60 0 0 -150)
RM3 36 38 50m
LM3 38 39 265u
Vout3 39 123 sin(0 196 60 0 0 -270)
*subcircuit for comparator
.subckt comp 1 2 9 10
rin 1 3 2.8k
r1 3 2 20meg
e2 4 2 3 2 50
r2 4 5 1k
d1 5 6 zenerdiode1
d2 2 6 zenerdiode2
e3 7 2 5 2 1
r3 7 8 10
c3 8 2 10n
r4 3 8 100k
e4 9 10 8 2 1
*models for zener diodes
.model zenerdiode1 D (Is=1p BV=0.1)
.model zenerdiode2 D (Is=1p BV=50)
.ends comp
*model for switch
.model qfet nmos(level=3 gamma=0
kappa=0 tox=100n rs=42.69m kp=20.87u
l=2u
+ w=2.9 delta=0 eta=0 theta=0 vmax=0 xj=0
uo=600 phi=0.6
+ vto=3.487 rd=0.19 cbd=200n pb=0.8
mj=0.5 cgso=3.5n cgdo=100p rg=1.2 is=10f)
```

Table 4. PSpice input program for PWM inverter operation

vtria1 5 0 pulse(-10 10 0 86.5u 86.5u 0.6u 173.6u) *gating signals for upper switches xgs1 14 5 11 10 comp xgs2 24 5 21 20 comp xgs3 34 5 31 30 comp *gating signals for lower switches egs4 41 0 poly(1) (11,10) 50 -1 egs5 51 0 poly(1) (21,20) 50 -1 egs6 61 0 poly(1) (31,30) 50 -1 *Filter is deleted because PSpice is limited to 64 nodes	*model for diodes .model diode d(is=1p) *options to aid convergence .options abstol=0.01m chgtol=0.01m reltol=50m vntol=1m itl5=0 itl4=200 *transient analysis .tran 5u 350m 300m 5u *plotting of traces .probe *Fourier analysis .four 60 12 I(L_w1) .end

Table 4. PSpice input program for PWM inverter operation (continuation)

Φ= 90 º	$V_{rms\ l\text{-}n}$=139 V	$I_{rms\ ph}$=54.90 A	V_{DC}=375 V	I_{THDi}=3.14%	m=1.04
Φ= 60 º	$V_{rms\ l\text{-}n}$=139 V	$I_{rms\ ph}$=48.57 A	V_{DC}=368 V	I_{THDi}=2.97%	m=1.07
Φ= 30 º	$V_{rms\ l\text{-}n}$=139 V	$I_{rms\ ph}$=44.80 A	V_{DC}=360 V	I_{THDi}=3.17%	m=1.09
Φ= 0 º	$V_{rms\ l\text{-}n}$=139 V	$I_{rms\ ph}$=45.08 A	V_{DC}=388 V	I_{THDi}=3.13%	m=1.01
Φ= -30 º	$V_{rms\ l\text{-}n}$=139 V	$I_{rms\ ph}$=48.59 A	V_{DC}=410 V	I_{THDi}=2.71%	m=0.96
Φ= -60 º	$V_{rms\ l\text{-}n}$=139 V	$I_{rms\ ph}$=53.58 A	V_{DC}=415 V	I_{THDi}=2.80%	m=0.95
Φ= -90 º	$V_{rms\ l\text{-}n}$=139 V	$I_{rms\ ph}$=59.09 A	V_{DC}=415 V	I_{THDi}=2.20%	m=0.95

Table 5. Dependency of the input DC voltage V_{DC} of inverter as a function of the output power factor angle Φ (generator notation, where a positive Φ corresponds to underexcited operation absorbing reactive power from the grid and a negative Φ corresponds to overexcited operation supplying reactive power to the grid) is the angle between phase current of inverter $I_{rms\ ph}$ and line-to-neutral voltage $V_{rms\ l\text{-}n}$ of power system, and m is the modulation index of inverter

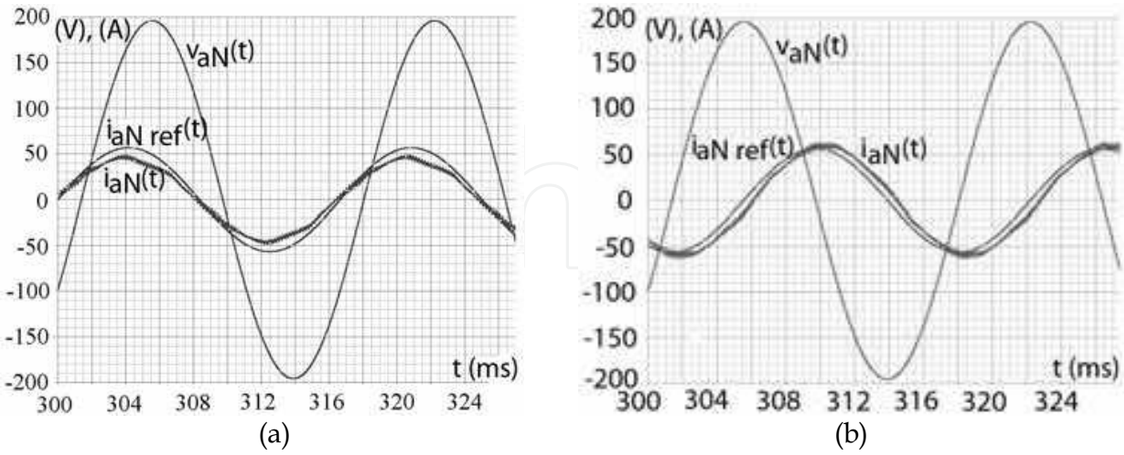

Figs. 13a,b. Inverter phase reference current, inverter phase output current, and power system phase voltage (about the same as inverter output voltage), see Fig.12a and Table 5; (a) Φ=30º (generator notation: leading power factor, underexcited, absorbing reactive power from grid); (b) Φ= - 90º (generator notation: lagging power factor, overexcited, delivering reactive power to grid)

3.2.4 Storage devices for short-term and long-term plants

Batteries, supercapacitors, ultracapacitors and flywheels serve as short-term storage devices while compressed air, flow batteries, (variable and constant-speed) hydro facilities and thermal storage are used for long-term storage facilities. Variable-speed WP and hydropower plants are based on the doubly-fed induction generator (DFIG) where energy can be provided under transient conditions by the rotating rotor slowing its angular velocity, and the DFIG may be used for short- and long-term storage. The required rotor excitation represents about 8% of the stator power (E.F. Fuchs & Masoum, 2011). Variable-speed drives (Yildirim *et al.*, 1998; E.F. Fuchs & Myat, 2010) are proposed for short- and long-term storage plants in order to eliminate mechanical gears.

4. Smartgrid and microgrids

Simultaneously, the implementation of smart/microgrids is accelerating. A key goal of SmartGrid City (Boulder, Colorado) and similar projects is to enable integration of significantly higher penetrations of renewable resources, both in concentrated utility-scale plants and dispersed residential-scale units. In addition to advanced utility controls such as smart meters, SmartGrid City combines a range of renewable resources. Specifically within Boulder, several hundred residential PV plants ranging from 2-10 kW are interconnected with the grid. Xcel's system includes an 8 MW PV plant in Colorado's San Luis Valley with an additional 17 MW PV plant (under construction) by Xcel Energy and SunPower.

Xcel's major Colorado WP resources include: Ponnequin/Weld County, 32 MW; Ridgecrest/Peetz, 30 MW; Colorado Green/Lamar, 162 MW; Spring Canyon/Peetz, 60 MW; Peetz Table/Peetz, 200 MW; Logan Wind/Peetz, 200 MW; Twin Buttes/Lamar, 75 MW; Cedar Creek/Grover, 300 MW; and Northern Colorado Wind/Peetz, 174 MW.

The Boulder municipal hydroelectric system includes 7 small hydropower plants generating more than 20,000 MWh per year (Cowdrey, 2004); these plants can operate intermittently depending upon the municipal treated water needs. Xcel also operates several pumped-storage (hydroelectric) plants, which can be relied upon for long-term storage. As a comparison Xcel's total installed power capacity in Colorado is 7 GW.

The smartgrid vision is the development of a smart (e.g., self-learning, self-healing, optimized, efficient, high power quality) power system, relying on existing proven distribution system technologies, adding new control and energy source/storage paradigms, and discarding approaches which interfere with intelligent control strategies, distributed generation and renewable resources. The smartgrid as envisioned by utilities must satisfy steady-state and transient operating conditions, avoiding the weak system effects (e.g., flicker, high-system impedance, voltage breakdown) encountered by the Danish grid, which has high WP plant penetration.

The rationale for the smart/microgrid lies in the integrative analysis of distributed energy sources--many of which will be intermittently operating--with the deployment of short-term and long-term storage plants. However, current load-sharing strategies will not work to integrate renewable sources and present-day storage plants because of the intermittent (peak-power) operation of renewable sources, and the online response time of different storage plants (E.F. Fuchs & Masoum, 2008a; E.F. Fuchs & Masoum, 2011). In addition, Fig. 4b illustrates that load-sharing utilizing standard droop strategies between two similarly-sized (e.g., PV) plants results in unstable frequency control due to similar response characteristics.

5. Design of short-term storage plants

Example # 4: Design a 10 MWh supercapacitor short-term storage plant

Relying solely on wind/solar energy is problematic because it may not be available when needed. A wind farm, for example, can lose as much as 60 MW within one minute. There are several scenarios of how the power change of 60 MW per minute can be mitigated through complementary, albeit more expensive, power sources. One is the combination of a (long-term) compressed-air storage (CAES) power plant with a (short-term) supercapacitor plant for bridging the time from when the WP plant output decreases (60 MW per minute) to when either a CAES plant (Mattick et al., 1975 and Vosburgh, 1978) or a pump-storage hydro plant (Glems, 1964; Raccoon Mountain, 1975; Cowdrey, 2004) can take over. A CAES plant requires a start-up time of about 6 minutes.

To bridge this 6-minute gap for a 100 MW compressed-air power plant, a supercapacitor plant can provide up to 100 MW during a 6-minute interval amounting to a required energy storage of 10 MWh. Inverters fed from a supercapacitor can deliver power within a few 60 Hz cycles to the power system, replacing the lost power of 60 MW per minute almost instantaneously. This combination of CAES plant and supercapacitor storage plant as a bridging energy source can be employed for peak-power operation as well as for improving power quality by preventing brownouts/blackouts. Fig. 14 depicts the block diagram of such a supercapacitor storage plant consisting of wind turbine, mechanical gear, synchronous generator, 3-phase transformer, 3-phase rectifier, supercapacitor bank, three-phase inverter, 3-phase transformer, and power system as discussed in Application Example 12.23 of (E.F. Fuchs & Masoum, 2011).

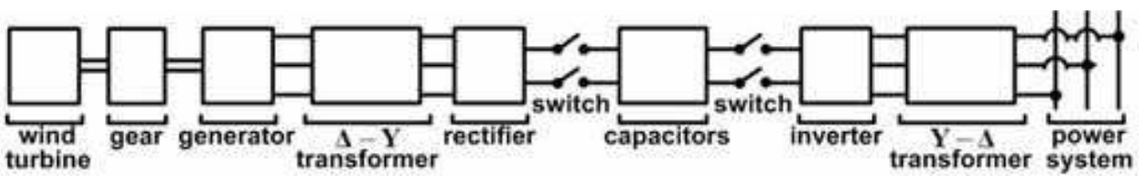

Fig. 14. Block diagram for charging and discharging supercapacitor bank

Example 5: Design of a 10MWh flywheel short-term storage power plant

Design a flywheel storage system which can provide for 6 minutes 100 MW, that is, energy of 10 MWh. The flywheel power plant consists (see Figs. 15a,b) of a flywheel, mechanical gear, synchronous machine, inverter-rectifier set and a step-up transformer (not shown in Fig. 15a). The individual components of this plant must be designed as follows: For the flywheel (made from steel) as shown in Fig. 15b (h=0.9 m, R_{1o}=1.5 m, R_{1i}=1.3 m, R_{2o}=0.50 m, R_{2i}=0.10 m, b=0.2 m), compute the energy stored as a function of angular velocity, see Application Example 12.26 of (E.F. Fuchs & Masoum, 2011).

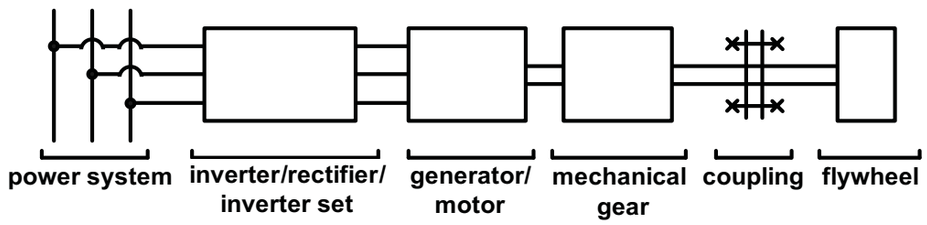

(a)

Fig. 15a. Flywheel power plant.

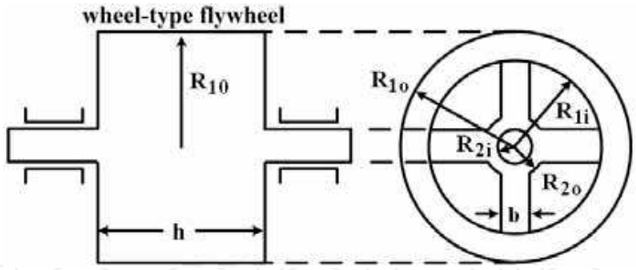

(b)

Fig. 15b. Flywheel power plant.

6. Complementary operation of renewable plants with short-term and long-term storage plants analyzed with either Mathematica or Matlab

The stability of a smart/microgrid consisting of a natural gas-fired power plant (the frequency leader), a long-term storage power plant, and two intermittently operating plants (i.e., PV and WP plants) with associated short-term storage plants is the objective of this section. In order to achieve stability for a given smart/micro- grid the following constraints must be satisfied:

1. instability and frequency variation is minimized through appropriate switching (in and out) of the short-term storage plants; in particular the time instant of switching is important.
2. transmission line (e.g., tie lines) parameters are optimized;
3. time constants of the governors and the valves must be within a feasible region;
4. droop characteristics of the individual plants must satisfy certain constraints.

Example 6: Operation of natural-gas fired and long-term storage plants with two renewable sources and two associated complementary short-term storage plants

Fig. 16 illustrates the sharing (increase) of the additional power among a short-term storage plant (e.g., R_2=0.01), a long-term-storage plant (e.g., R_3=10), and a PV plant (e.g., R_1=10) causing a frequency decrease. Stable frequency control is obtained when the short-term storage plant compensates the intermittent power output of the PV plant, and the plant with spinning reserve of Fig. 2 (natural-gas fired plant) is replaced by a long-term storage plant which is connected all the time to the power system and serves in this case as frequency leader. The PV plant and the short-term storage plant may operate intermittently but only in a complementary fashion.

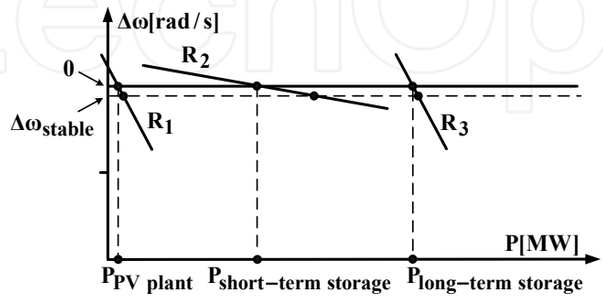

Fig. 16. Drooping characteristics of the short-term storage plant (e.g., R_2=0.01), the long-term storage plant (e.g., R_3=10), and intermittently operating PV (e.g., R_1=10) plant, accommodating additional demand/increase of power, where the PV plant is operated at peak power and cannot deliver additional power.

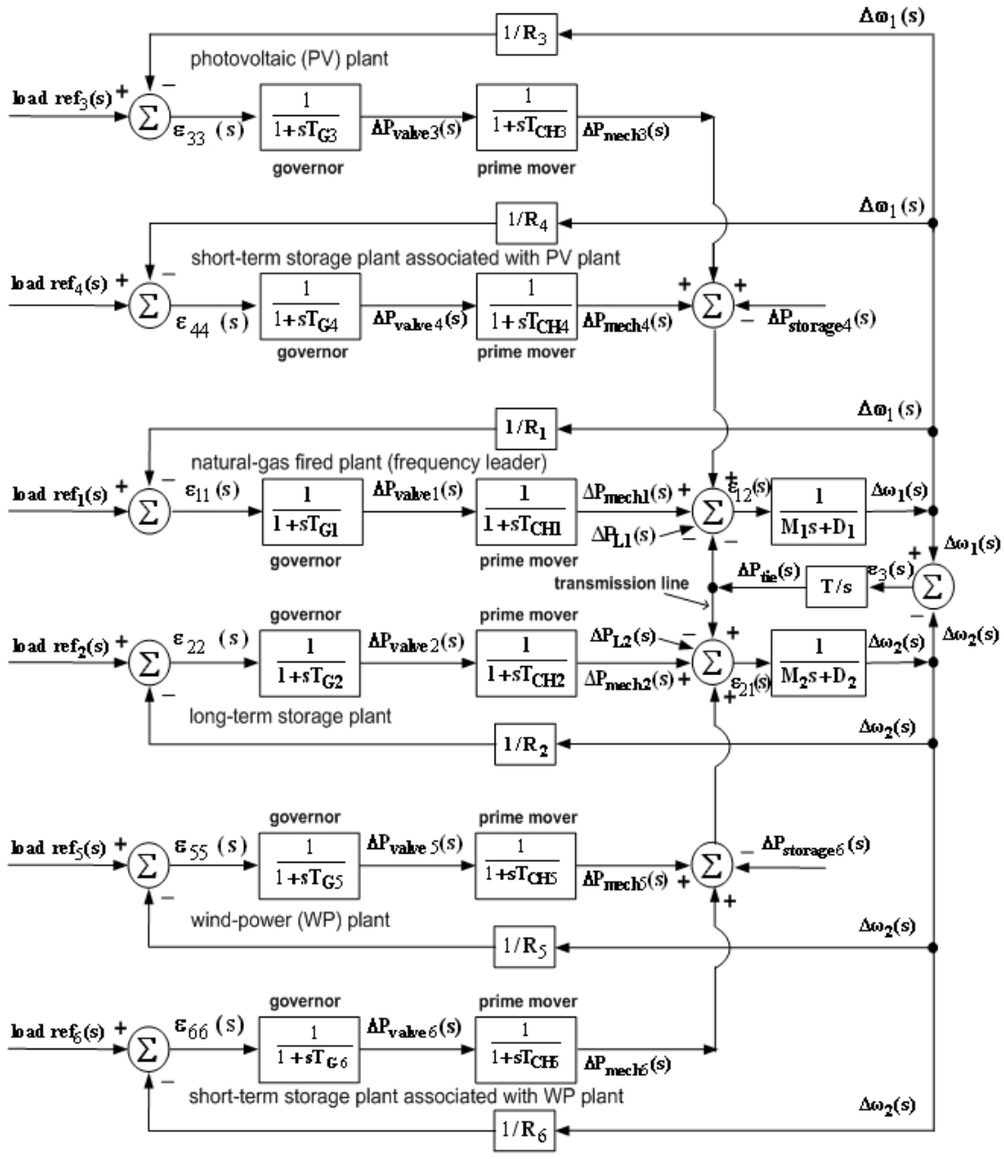

Fig. 17a. Block diagram of smart/micro grid resulting in stable frequency control.

In Fig. 2 the spinning reserve plant can be replaced by a natural-gas fired plant and a long-term storage plant (e.g., pump-hydro or compressed air facility), as shown in Figs. 17a, b, c. The intermittently operating PV and WP plants are complemented by short-term storage plants (e.g., battery-fed inverter). During times of high power demand, the storage plants supply power to maintain the power balance between generation and the served loads. At low power demand, the renewable sources will supply the storage plants. The generation increase of conventional peak-power plants (which can supply additional load through spinning reserve) are replaced by putting short-term (located next to renewable plants) and long-term storage plants (E.F. Fuchs & Masoum, 2008a, E.F. Fuchs & Masoum, 2011) online, reducing fossil-fuel consumption and contributing to renewable portfolio standards. Renewable sources are operated at their peak-power point e.g., the slopes of the droop characteristic R_3 and R_5 of Fig. 17b are large while those of R_1 and R_2 are relatively small to

permit the increase of their output power upon demand. Thus the PV and WP plants cannot participate in frequency/load control. In Figu. 17c, all droop characteristics have a relatively small slope and all participating plants can output increased power and participate in frequency/load control. In the block diagram of the PV plant of Fig. 17a the governor and prime mover represent the solar array and inverter/rectifier while in the short-term storage plant associated with the PV plant, the governor and prime mover represent the storage device (e.g., battery, supercapacitor, flywheel) and inverter/rectifier. Similar considerations apply to the WP plant and its associated short-term storage plant.

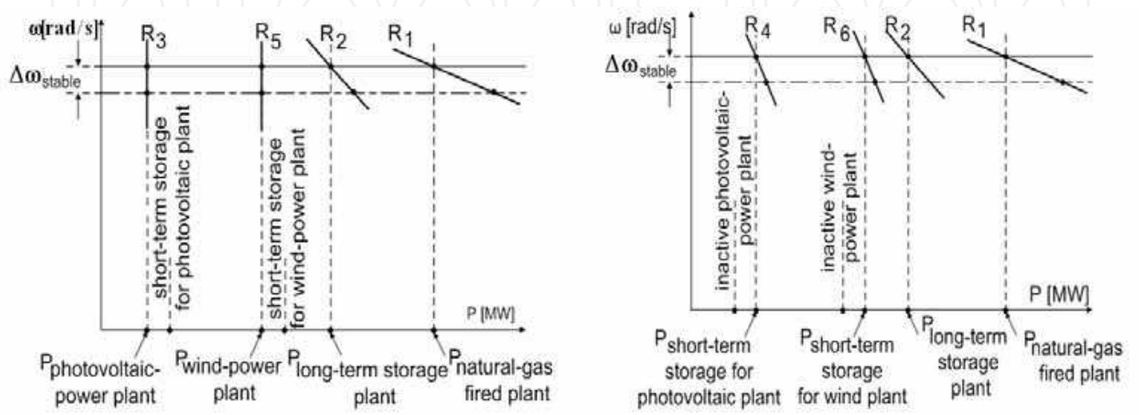

(b) (c)

Figs. 17b,c. The natural-gas fired plant serves as frequency leader and the long-term storage plant serves as spinning reserve; (b) PV and WP plants operate at peak power and storage plants are disconnected; (c) Short-term storage plants compensate the zero power outputs of the PV and WP plants.

Data for natural-gas fired plant (system #1 of Fig.17a): Angular frequency per-unit (pu) change $\Delta\omega_1$ per change in generator output power ΔP_1, that is, $R_1=\Delta\omega_1/\Delta P_1=0.01$ pu, the frequency-dependent load change ΔP_{L1_frequ} per angular frequency change $\Delta\omega_1$, that is, $D_1=\Delta P_{L1\_frequ}/\Delta\omega_1=0.8$ pu, positive step-load change $\Delta P_{L1}/s=0.1/s$ pu, angular momentum of gas turbine and generator set $M_1=4.5$, base apparent power $S_{base}=500$ MVA, governor time constant $T_{G1}=0.3$ s, valve changing/charging time constant $T_{CH1}=0.9$ s, and load $ref_1(s)=0.8$ pu.
Data for long-term storage plant (system #2 of Fig.17a): Angular frequency per-unit (pu) change $\Delta\omega_2$ per change in generator output power ΔP_2, that is, $R_2=\Delta\omega_2/\Delta P_2=0.1$ pu (e.g., variable-speed pump hydropower plant), the frequency-dependent load change ΔP_{L2_frequ} per angular frequency change $\Delta\omega_2$, that is, $D_2=\Delta P_{L2\_frequ}/\Delta\omega_2=1.0$ pu, negative step-load change $\Delta P_{L2}(s)=\Delta P_{L2}/s=-0.2/s$ pu, angular momentum of hydro turbine and generator set $M_2=6$, base apparent power $S_{base}=500$ MVA, governor time constant $T_{G2}=0.2$ s, valve changing/charging time constant $T_{CH2}=0.2$ s, and load $ref_2(s)=0.5$ pu.
Data for tie line: $T=\omega_o/X_{tie}$ with $X_{tie}=0.2$ pu and $\omega_o=377$ rad/s for f=60Hz.
Data for PV plant (system #3 of Fig.17a): Angular frequency change $\Delta\omega_1$ per change in inverter output power ΔP_3, that is, $R_3=\Delta\omega_1/\Delta P_3=0.3$ pu, governor time constant $T_{G3}=0.1$ s, equivalent valve time constant $T_{CH3}=0.1$ s, and load $ref_3(s)=0.01$ pu.
Data for short-term storage plant associated with PV plant (system #4 of Fig.17a): Angular frequency change $\Delta\omega_1$ per change in generator output power ΔP_4, that is, $R_4=\Delta\omega_1/\Delta P_4=0.5$ pu, governor time constant $T_{G4}=0.2$ s, equivalent valve time constant $T_{CH4}=0.1$ s, and load $ref_4(s)=0.01$ pu.

Data for WP plant (system #5 of Fig.17a): Angular frequency change $\Delta\omega_2$ per change in generator output power ΔP_5, that is, $R_5=\Delta\omega_2/\Delta P_5=0.7$ pu, governor time constant $T_{G5}=0.1$ s, equivalent valve time constant $T_{CH5}=0.1$ s, and load $ref_5(s)=0.01$ pu.
Data for short-term storage plant associated with WP plant (system #6 of Fig.17a): Angular frequency change $\Delta\omega_2$ per change in generator output power ΔP_6, that is, $R_6=\Delta\omega_2/\Delta P_6=0.5$ pu, governor time constant $T_{G6}=0.2$ s, equivalent valve time constant $T_{CH6}=0.1$ s, and load $ref_6(s)=0.01$ pu.

a. List the ordinary differential equations and the algebraic equations of the block diagram of Fig. 17a. Derive the transfer function of the transmission (e.g., tie line) line.
b. Use either Mathematica or Matlab to establish steady-state conditions by imposing positive step functions for load $ref_1(s)=0.8/s$ pu, load $ref_2(s)=0.5/s$ pu, load $ref_3(s)=$ load $ref_4(s)=$ load $ref_5(s)=$ load $ref_6(s)=0.01/s$ pu, and run the program with a zero step-load changes $\Delta P_{L1}=0$, $\Delta P_{L2}=0$ for 200 s. Save the steady-state values for all variables at 200 s. Plot the calculated angular frequency response $\Delta\omega(t)$ [pu]= $\Delta\omega_1(t)$ [pu]= $\Delta\omega_2(t)$ [pu].
c. Initialize the parameters with the steady-state values as obtained in Part b). After 300 s impose positive step-load change $\Delta P_{L1}(s)=\Delta P_{L1}/s=0.1/s$ pu, and after 400 s impose negative step-load change $\Delta P_{L2}(s)=\Delta P_{L2}/s=-0.1/s$ pu. Thereafter, for load $ref_3(s)$, load $ref_4(s)$, load $ref_3(s)$, load $ref_5(s)$, $DPstorage_4(s)$, $DPstorage_6(s)$ and load $ref_4(s)$:
   Lr3[t_]:=If [t<600, 0, 0.06];
   Lr4[t_]:=If [t<600.1, 0,- 0.6];
   Lr3[t_]:=If [t<1200,If[t<1120,If[t<1000,If[t<940,If[t<910,0,0.03],0.09],0.05],0.03],0.0];
   Lr5[t]:=If [t<1200,If[t<1120,If[t<1000,If[t<940,If[t<910,0,0.3],0.9],0.5],0.3],0.0];
   DPstorage4[t_]:=If[t<1200.2,If[t<1120.2,If[t<1000.2,If[t<940.2,If[t<910.2,0,0.15],0.45],0.25],0.15],0.0];
   DPstorage6[t_]:=If[t<1200.2,If[t<1120.2,If[t<1000.2,If[t<940.2,If[t<910.2,0,0.15],0.45],0.25],0.15],0.0];
   Lr4[t_]:=If [t<700, 0,- 0.01].
   Plot the given WP plant load reference Lr5[t] and calculated the transient response $\Delta\omega(t)$ for a total of 1,500 s.
d. Initialize the parameters with the steady-state values as obtained in Part b). After 300 s impose positive step-load change $\Delta P_{L1}(s)=\Delta P_{L1}/s=0.1/s$ pu, and after 400 s impose negative step-load change $\Delta P_{L2}(s)=\Delta P_{L2}/s=-0.1/s$ pu. Thereafter:
   Lr3[t_]:=If [t<600, 0, 0.6];
   Lr4[t_]:=If [t<600.1, 0,- 0.6];
   Lr3[t_]:=If [t<1200,If[t<1120,If[t<1000,If[t<940,If[t<910,0,0.03],0.09],0.05],0.03],0.0];
   Lr5[t_]:=If [t<1200,If[t<1120,If[t<1000,If[t<940,If[t<910,0,0.3],0.9],0.5],0.3],0.0];
   DPstorage4[t_]:=If[t<1200.2,If[t<1120.2,If[t<1000.2,If[t<940.2,If[t<910.2,0,0.01],0.01],0.01],0,0.01],0.0];
   DPstorage6[t_]:=If[t<1200.2,If[t<1120.2,If[t<1000.2,If[t<940.2,If[t<910.2,0,0.30],0.90],0.50],0.30],0.0];
   Lr4[t_]:=If [t<700, 0,- 0.3].
   Calculate and plot the transient response $\Delta\omega(t)$ for a total of 1,500 s.
e. Initialize the parameters with the steady-state values as obtained in Part b). After 300 s impose positive step-load change $\Delta P_{L1}(s)=\Delta P_{L1}/s=0.1/s$ pu, and after 400 s impose negative step-load change $\Delta P_{L2}(s)=\Delta P_{L2}/s=-0.1/s$ pu. Thereafter:

Lr3[t_]:=If [t<600, 0, 0.6];
Lr4[t_]:=If [t<600.1, 0,- 0.6];
Lr3[t_]:=If [t<1200,If[t<1120,If[t<1000,If[t<940,If[t<910,0,0.03],0.09],0.05],0.03],0.0];
Lr5[t_]:=If [t<1200,If[t<1120,If[t<1000,If[t<940,If[t<910,0,0.3],0.9],0.5],0.3],0.0];
DPstorage4[t_]:=If[t<1205.2,If[t<1125.2,If[t<1005.2,If[t<950.2,If[t<920.2,0,0.30],0.90],0.50],0.30],0.0];
DPstorage6[t_]:=If[t<1200.2,If[t<1120.2,If[t<1000.2,If[t<940.2,If[t<910.2,0,0.01],0.01],0.01],0,0.01],0.0];
Lr4[t_]:=If [t<700, 0,- 0.3].
Calculate and plot the transient response $\Delta\omega(t)$ for a total of 1,500 s.

f. Initialize the parameters with the steady-state values as obtained in Part b). After 300 s impose positive step-load change $\Delta P_{L1}(s)=\Delta P_{L1}/s=0.1/s$ pu, and after 400 s impose negative step-load change $\Delta P_{L2}(s)=\Delta P_{L2}/s = - 0.1/s$ pu. Thereafter:
Lr3[t_]:=If [t<600, 0, 0.6];
Lr4[t_]:=If [t<600.1, 0,- 0.6];
Lr3[t_]:=If[t<1200,If[t<1120,If[t<1000,If[t<940,If[t<910,0,0.03],0.09],0.05],0.03],0.0];
Lr5[t_]:=If [t<1200,If[t<1120,If[t<1000,If[t<940,If[t<910,0,0.3],0.9],0.5],0.3],0.0];
DPstorage4[t_]:=If[t<1230,If[t<1150,If[t<1030,If[t<970,If[t<940,0,0.030],0.090],0.050],0.030],0.0];
DPstorage6[t_]:=If[t<1200.2,If[t<1120.2,If[t<1000.2,If[t<940.2,If[t<910.2,0,0.01],0.01],0.01],0,0.01],0.0];
Lr4[t_]:=If [t<700, 0,- 0.3].
Calculate and plot the transient response $\Delta\omega(t)$ for a total of 1,500 s.

g. Investigate the influence of the power capability of the transmission line for the conditions as given in part c) by increasing X_{tie} from 0.2 pu to 0.237 pu.

Solution:

a. Differential and algebraic equations:
System #1: ε_{11}=load $ref_1-\Delta\omega_1/R_1$, $\Delta P_{valve\_1}+T_{G1}d(\Delta P_{valve\_1})/dt=\varepsilon_{11}$, $\Delta P_{mech\_1}+ T_{CH1}d(\Delta P_{mech\_1})/dt =\Delta P_{valve\_1}$, $\varepsilon_{12}=\Delta P_{mech\_1}-\Delta P_{L1}-\Delta P_{tie}+\Delta P_{mech\_3}+\Delta P_{mech\_4}-\Delta P_{storage\_4}$, $\Delta\omega_1 D_1+M_1 d(\Delta\omega_1)/dt=\varepsilon_{12}$.
Coupling (tie, transmission) network: $(1/T)d(\Delta P_{tie})/dt=\varepsilon_3$, where $\varepsilon_3=\Delta\omega_1-\Delta\omega_2$.
System #2: ε_{22}=load $ref_2-\Delta\omega_2/R_2$, $\Delta P_{valve\_2}+T_{G2}d(\Delta P_{valve\_2})/dt=\varepsilon_{22}$, $\Delta P_{mech\_2}+T_{CH2}d(\Delta P_{mech\_2})/dt=\Delta P_{valve\_2}$, $\varepsilon_{21}=\Delta P_{mech\_2}-\Delta P_{L2}+\Delta P_{tie}+\Delta P_{mech\_5}+\Delta P_{mech\_6}-\Delta P_{storage\_6}$, $\Delta\omega_2 D_2+M_2 d(\Delta\omega_2)/dt=\varepsilon_{21}$.
System #3: ε_{33}=load $ref_3-\Delta\omega_1/R_3$, $\Delta P_{valve\_3}+T_{G3}d(\Delta P_{valve\_3})/dt=\varepsilon_{33}$, $\Delta P_{mech\_3}+T_{CH3}d(\Delta P_{mech\_3})/dt =\Delta P_{valve\_3}$.
System #4: ε_{44}=load $ref_4-\Delta\omega_1/R_4$, $\Delta P_{valve\_4}+T_{G4}d(\Delta P_{valve\_4})/dt=\varepsilon_{44}$, $\Delta P_{mech\_4}+T_{CH4}d(\Delta P_{mech\_4})/dt =\Delta P_{valve\_4}$.
System #5: ε_{55}=load $ref_5-\Delta\omega_2/R_5$, $\Delta P_{valve\_5}+T_{G5}d(\Delta P_{valve\_5})/dt=\varepsilon_{55}$, $\Delta P_{mech\_5}+T_{CH5}d(\Delta P_{mech\_5})/dt =\Delta P_{valve\_5}$.
System #6: ε_{66}=load $ref_6-\Delta\omega_2/R_6$, $\Delta P_{valve\_6}+T_{G6}d(\Delta P_{valve\_6})/dt=\varepsilon_{66}$, $\Delta P_{mech\_6}+T_{CH6}d(\Delta P_{mech\_6})/dt =\Delta P_{valve\_6}$.
Derivation of the tie-line transfer function:
The real power flow from bus # 1 with voltage $\tilde{V}_1$ to bus #2 with voltage $\tilde{V}_2$ is for the line reactance X_{line} neglecting the line resistance R_{line}: $P_{tie}=\dfrac{|\tilde{V}_1||\tilde{V}_2|}{X_{line}}\sin\theta$, where θ is the

angle between $\tilde{V}_1$ and $\tilde{V}_2$. For $|\tilde{V}_1| \approx |\tilde{V}_2|$ =constant their perturbations are $|\Delta\tilde{V}_1|$ = $|\Delta\tilde{V}_2|$ =0. Introducing perturbations for P and θ one obtains

$$P_{tieo} + \Delta P_{tie} = \frac{|\tilde{V}_{1o}||\tilde{V}_{2o}|}{X_{line}} \sin(\theta_o + \Delta\theta) = \frac{|\tilde{V}_{1o}||\tilde{V}_{2o}|}{X_{line}} \sin(\theta_o \cos\Delta\theta + \cos\theta_o \sin\Delta\theta) \quad (3)$$

$$P_{tieo} = \frac{|\tilde{V}_{1o}||\tilde{V}_{2o}|}{X_{line}} \sin\theta_o \text{ and } \Delta P_{tie} = \frac{|\tilde{V}_{1o}||\tilde{V}_{2o}|}{X_{line}} \cos(\theta_o)\,\Delta\theta = \frac{|\tilde{V}_{1o}||\tilde{V}_{2o}|}{X_{line}/\cos(\theta_o)}\,\Delta\theta = \frac{|\tilde{V}_{1o}||\tilde{V}_{2o}|}{X_{tie}}\,\Delta\theta$$

$$\Delta P_{tie} = \frac{|\tilde{V}_{1o}||\tilde{V}_{2o}|}{d(X_{tie})/dt}\, d(\Delta\theta)/dt, \text{ where } X_{tie} = X_{line}/\cos\theta o \quad (4)$$

or with the Laplace operator s=d(…)/dt

$$\Delta P_{tie} = \frac{|\tilde{V}_{1o}||\tilde{V}_{2o}|}{sX_{tie}}\,\Delta\omega(s) = \frac{|\tilde{V}_{1o}||\tilde{V}_{2o}|}{sX_{tie}}\,\{\Delta\omega_1(s) - \Delta\omega_2(s)\}. \quad (5)$$

In per unit with V_{base}, Z_{base} and $\omega_o = 2\pi f = 377$ rad/s as references one obtains with $T = T_{tie} = \omega_o[\text{rad/s}]/X_{tie}[\text{pu}] = 377/X_{tie}[\text{pu}]$ for f=60 Hz.

$$\Delta P_{tie}[\text{pu}] = (T/s)\{\Delta\omega_1(s)[\text{pu}] - \Delta\omega_2(s)[\text{pu}]\}. \quad (6)$$

The frequency variation of a power system should be within 59-61 Hz, that is, a frequency band of ±1.66 Hz is desirable (Fuller *et al.*, 1989). Table 6 lists the Mathematica program for Fig. 17a on which Figs. 18 and 19 are based.

b. Fig. 18a illustrates the establishment of steady-state conditions at time t=200 s for given systems parameters.

c. Fig. 18b illustrates the given WP plant load reference Lr5[t]. Fig.18c shows the transient response Δω(t) if storage plants 4 and 6 absorb the additional energy generated by WP plant with 0.2 s delay (see Table 6).

R1=0.01;	DPvalve4b=(DPvalve4[t]/.sol1[[1]]/.t->200);
d1=0.8;	DPmech5b=(DPmech5[t]/.sol1[[1]]/.t->200);
M1=4.5;	DPvalve5b=(DPvalve5[t]/.sol1[[1]]/.t->200);
Tg1=0.3;	DPmech6b=(DPmech6[t]/.sol1[[1]]/.t->200);
Tch1=0.9;	DPvalve6b=(DPvalve6[t]/.sol1[[1]]/.t->200);
Lr1=0.8;	ic16=Dw1[200]=Dw1b;
DPL1[t_]:=If [t<210, 0, 0.1];	ic17=DPmech1[200]=DPmech1b;
R2=0.1;	ic18=DPvalve1[200]=DPvalve1b;
d2=1.0;	ic19=DPtie[200]=DPtie1b;
M2=6;	ic20=Dw2[200]=Dw2b;
Tg2=0.2;	ic21=DPmech2[200]=DPmech2b;

Table 6. Mathematica input program for stability analysis of Figs. 17-19

```
Tch2=0.2;
Lr2=0.5;
DPL2[t_]:=If [t<400, 0, -0.1];
Xtie=0.2;
Ttie=377/Xtie;
R3=0.3;
Tg3=0.1;
Tch3=0.1;
Lr3[t_]:=If [t<600, 0, 0.06];
R4=0.5;
Tg4=0.2;
Tch4=0.1;
Lr4[t_]:=If [t<600.1, 0,- 0.6];
R5=0.7;
Tg5=0.1;
Tch5=0.1;
Lr5[t]:=If [t<600.2, 0, 0.3];
R6=0.5;
Tg6=0.2;
Tch6=0.1;
Lr6=0.01;
ic1=Dw1[0]= =0;
ic2=DPmech1[0]= =0;
ic3=DPvalve1[0]= =0;
ic4=DPtie[0]= =0;
ic5=Dw2[0]= =0;
ic6=DPmech2[0]= =0;
ic7=DPvalve2[0]= =0;
ic8=DPmech3[0]= =0;
ic9=DPvalve3[0]= =0;
ic10=DPmech4[0]= =0;
ic11=DPvalve4[0]= =0;
ic12=DPmech5[0]= =0;
ic13=DPvalve5[0]= =0;
ic14=DPmech6[0]= =0;
ic15=DPvalve6[0]= =0;
E11[t_]:=Lr1-Dw1[t]/R1;
E12[t_]:=DPmech1[t]-DPL1[t]-
DPtie[t]+ DPmech3[t]+DPmech4[t];
E3[t_]:=Dw1[t]-Dw2[t];
E22[t_]:=Lr2-Dw2[t]/R2;
E21[t_]:=DPmech2[t]-
DPL2[t]+DPtie[t]                +
DPmech5[t]+DPmech6[t];
E33[t_]:=Lr3[t]-Dw1[t]/R3;
ic22=DPvalve2[200]=DPvalve2b;
ic23=DPmech3[200]=DPmech3b;
ic24=DPvalve3[200]=DPvalve3b;
ic25=DPmech4[200]=DPmech4b;
ic26=DPvalve4[200]=DPvalve4b;
ic27=DPmech5[200]=DPmech5b;
ic28=DPvalve5[200]=DPvalve5b;
ic29=DPmech6[200]=DPmech6b;
ic30=DPvalve6[200]=DPvalve6b;
R1=0.01;
d1=0.8;
M1=4.5;
Tg1=0.3;
Tch1=0.9;
Lr1=0.8;
DPL1[t_]:=If [t<300, 0, 0.1];
R2=0.1;
d2=1.0;
M2=6;
Tg2=0.2;
Tch2=0.2;
Lr2=0.5;
DPL2[t_]:=If [t<400, 0, -0.1];
Xtie=0.2;
Tie=377/Xtie;
R3=0.3;
Tg3=0.1;
Tch3=0.1;
Lr3[t_]:=If[t<1200,If[t<1120,If[t<1000,If[t<940,
If[t<910,0,0.03],0.09],0.05],0.03],0.0];
DPstorage4[t_]:=If[t<1200.2,If[t<1120.2,If[t<1000
.2,
If[t<940.2,If[t<910.2,0,0.15],0.45],0.25],0.15],0.0];
DPstorage6[t_]:=If[t<1200.2,If[t<1120.2,If[t<1000
.2,
If[t<940.2,If[t<910.2,0,0.15],0.45],0.25],0.15],0.0];
R4=0.5;
Tg4=0.2;
Tch4=0.1;
Lr4[t_]:=If [t<700, 0,- 0.01];
R5=0.7;
Tg5=0.1;
Tch5=0.1;
Lr5[t]:=If [t<1200,If[t<1120,If[t<1000,If[t<940,
If[t<910,0,0.3],0.9],0.5],0.3],0.0];
```

Table 6. Mathematica input program for stability analysis of Figs. 17-19 (continuation)

```
E44[t_]:=Lr4[t]-Dw1[t]/R4;
E55[t_]:=Lr5[t]-Dw2[t]/R5;
E66[t_]:=Lr6-Dw2[t]/R6;
eqn1=Dw1'[t]= =(1/M1)*(E12[t]-d1*Dw1[t]);
eqn2=DPmech1'[t]= =(1/Tch1)*(DPvalve1[t]-DPmech1[t]);
eqn3=DPvalve1'[t]= =(1/Tg1)*(E11[t]-DPvalve1[t]);
eqn4=DPtie'[t]= =Tie*E3[t];
eqn5=Dw2'[t]= =(1/M2)*(E21[t]-d2*Dw2[t]);
eqn6=DPmech2'[t]= =(1/Tch2)*(DPvalve2[t]-DPmech2[t]);
eqn7=DPvalve2'[t]= =(1/Tg2)*(E22[t]-DPvalve2[t]);
eqn8=DPmech3'[t]= =(1/Tch3)*(DPvalve3 [t]-DPmech3[t]);
eqn9=DPvalve3'[t]= =(1/Tg3)*(E33[t]-DPvalve3[t]);
eqn10=DPmech4'[t]= =(1/Tch4)*(DPvalve4[t]-DPmech4[t]);
eqn11=DPvalve4'[t]= =(1/Tg4)*(E44[t]-DPvalve4[t]);
eqn12=DPmech5'[t]= =(1/Tch5)*(DPvalve5 [t]-DPmech5[t]);
eqn13=DPvalve5'[t]= =(1/Tg5)*(E55[t]-DPvalve5[t]);
eqn14=DPmech6'[t]= =(1/Tch6)*(DPvalve6[t]-DPmech6[t]);
eqn15=DPvalve6'[t]= =(1/Tg6)*(E66[t]-DPvalve6[t]);
sol1=NDSolve[{eqn1,eqn2,eqn3,eqn4,eqn5,eqn6,eqn7,eqn8,eqn9,eqn10,eqn11
,eqn12,eqn13,eqn14,eqn15,ic1,ic2,ic3,ic4
,ic5,ic6,ic7,ic8,ic9,ic10,ic11,ic12,ic13,ic14,
ic15},{Dw1[t],DPmech1[t],DPvalve1[t],
DPtie[t],Dw2[t],DPmech2[t],Dpval
ve2[t],DPmech3[t],DPvalve3[t],DPmech
4[t],DPvalve4[t],DPmech5[t],Dpvalv
e5[t],DPmech6[t],DPvalve6[t]},{t,0,200
},MaxSteps->100000000];
Plot[Dw1[t]/.sol1[[1]],{t,0,200},PlotRa
nge->All,AxesLabel-
>{"t[s]","Dw1[t][pu]"}]
```

```
R6=0.5;
Tg6=0.2;
Tch6=0.1;
Lr6=0.01;
E11[t_]:=Lr1-Dw1[t]/R1;
E12[t_]:=DPmech1[t]-DPL1[t]-DPtie[t]+
DPmech3[t]+DPmech4[t]-DPstorage4[t];
E3[t_]:=Dw1[t]-Dw2[t];
E22[t_]:=Lr2-Dw2[t]/R2;
E21[t_]:=DPmech2[t]-DPL2[t]+DPtie[t] +
DPmech5[t]+DPmech6[t]-DPstorage6[t];
E33[t_]:=Lr3[t]-Dw1[t]/R3;
E44[t_]:=Lr4[t]-Dw1[t]/R4;
E55[t_]:=Lr5[t]-Dw2[t]/R5;
E66[t_]:=Lr6-Dw2[t]/R6;
eqn1=Dw1'[t]= =(1/M1)*(E12[t]-d1*Dw1[t]);
eqn2=DPmech1'[t]= =(1/Tch1)*(DPvalve1[t]-
DPmech1[t]);
eqn3=DPvalve1'[t]= =(1/Tg1)*(E11[t]-
DPvalve1[t]);
eqn4=DPtie'[t]= =Tie*E3[t];
eqn5=Dw2'[t]= =(1/M2)*(E21[t]-d2*Dw2[t]);
eqn6=DPmech2'[t]= =(1/Tch2)*(DPvalve2[t]-
DPmech2[t]);
eqn7=DPvalve2'[t]= =(1/Tg2)*(E22[t]-
DPvalve2[t]);
eqn8=DPmech3'[t]= =(1/Tch3)*(DPvalve3 [t]-
DPmech3[t]);
eqn9=DPvalve3'[t]= =(1/Tg3)*(E33[t]-
DPvalve3[t]);
eqn10=DPmech4'[t]= =(1/Tch4)*(DPvalve4[t]-
DPmech4[t]);
eqn11=DPvalve4'[t]= =(1/Tg4)*(E44[t]-
DPvalve4[t]);
eqn12=DPmech5'[t]= =(1/Tch5)*(DPvalve5 [t]-
DPmech5[t]);
eqn13=DPvalve5'[t]= =(1/Tg5)*(E55[t]-
DPvalve5[t]);
eqn14=DPmech6'[t]= =(1/Tch6)*(DPvalve6[t]-
DPmech6[t]);
eqn15=DPvalve6'[t]= =(1/Tg6)*(E66[t]-
DPvalve6[t]);
sol2=NDSolve[{eqn1,eqn2,eqn3,eqn4,eqn5,eqn6,
eqn7,eqn8,
eqn9,eqn10,eqn11,eqn12,eqn13,eqn14,eqn15,ic1,
```

Table 6. Mathematica input program for stability analysis of Figs. 17-19 (continuation)

Dw1b=(Dw1[t]/.sol1[[1]]/.t->200) DPmech1b=(DPmech1[t]/.sol1[[1]]/.t->200); DPvalve1b=(DPvalve1[t]/.sol1[[1]]/.t->200); DPtie1b=(DPtie[t]/.sol1[[1]]/.t->200); Dw2b=(Dw2[t]/.sol1[[1]]/.t->200) DPmech2b=(DPmech2[t]/.sol1[[1]]/.t->200); DPvalve2b=(DPvalve2[t]/.sol1[[1]]/.t->200); DPmech3b=(DPmech3[t]/.sol1[[1]]/.t->200); DPvalve3b=(DPvalve3[t]/.sol1[[1]]/.t->200); DPmech4b=(DPmech4[t]/.sol1[[1]]/.t->200);	ic2,ic3,ic4, ic5,ic6,ic7,ic8,ic9,ic10,ic11,ic12,ic13,ic14,ic15}, {Dw1[t], DPmech1[t],DPvalve1[t],DPtie[t],Dw2[t], DPmech2[t], DPvalve2[t],DPmech3[t],DPvalve3[t],DPmech4[t], DPvalve4[t], DPmech5[t],DPvalve5[t],DPmech6[t],DPvalve6[t]}, {t,200,1500}, MaxSteps->100000000]; Plot[Evaluate[Lr5[t]],{t,200,1500},PlotRange->All,AxesLabel->{"t (s)","Lr5[t] [pu]"}] Plot[Dw1[t]/.sol2[[1]],{t,200,1500},PlotRange->All,AxesLabel->{"t[s]","Dw1[t][pu]"}]

Table 6. Mathematica input program for stability analysis of Figs. 17-19 (continuation)

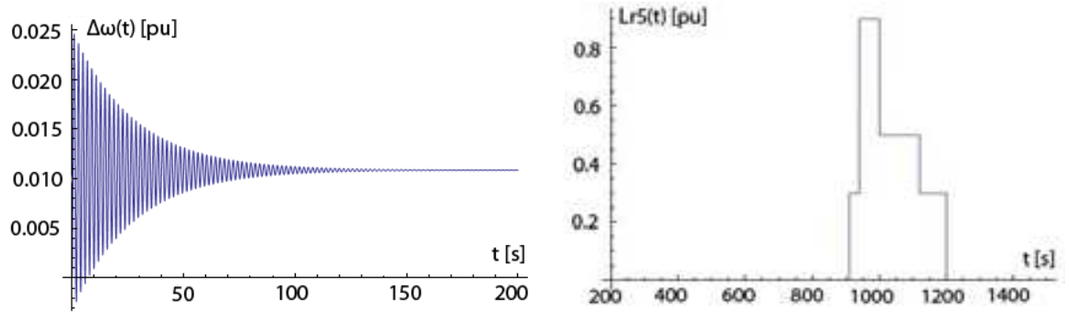

(a) (b)

Figs. 18a,b. (a) Establishment of steady-state conditions for Δω(t); (b) Plot of given WP plant load reference Lr5[t]

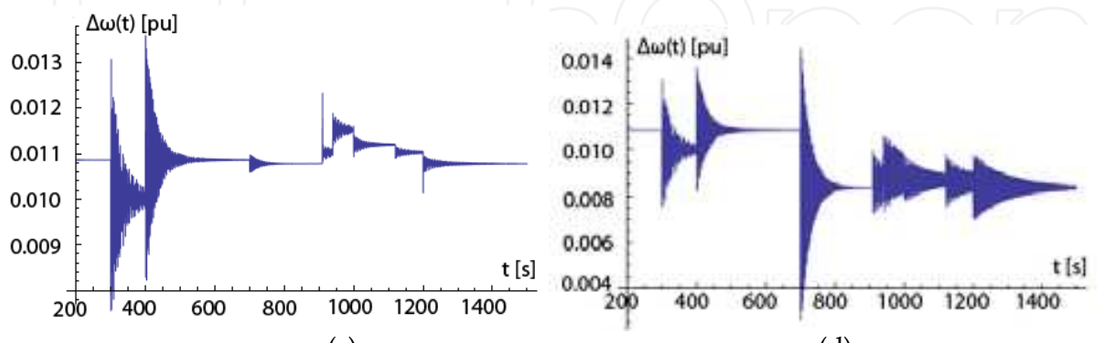

(c) (d)

Figs. 18c,d. (c) Transient response Δω(t) if storage plants 4 and 6 absorb the additional energy generated by WP plant with 0.2 s delay; (d) Transient response Δω(t) if only storage plant 6 absorbs the additional energy generated by WP plant with 0.2 s delay.

d. Fig. 18d depicts the transient response Δω(t) if only storage plant 6 absorbs the additional energy generated by WP plant with 0.2 s delay.
e. If the change of the WP plant is absorbed by the short-term storage plant 4 associated with the PV plant then Fig. 18e is obtained.
f. Fig. 18f shows the transient response Δω(t) if none of the storage plants absorbs a substantial amont of energy generated by WP plant.
g. Figs. 19a, b illustrate the influence of the reduction of the power capability of the transmission line increasing X_{tie} from 0.2 pu to 0.237 pu for the conditions of Fig.18c. Fig. 19a shows that steady-state stability is impaired, and after some load/demand changes the dynamic stability is lost (Fig. 19b) and the angular frequency/velocity diverges.

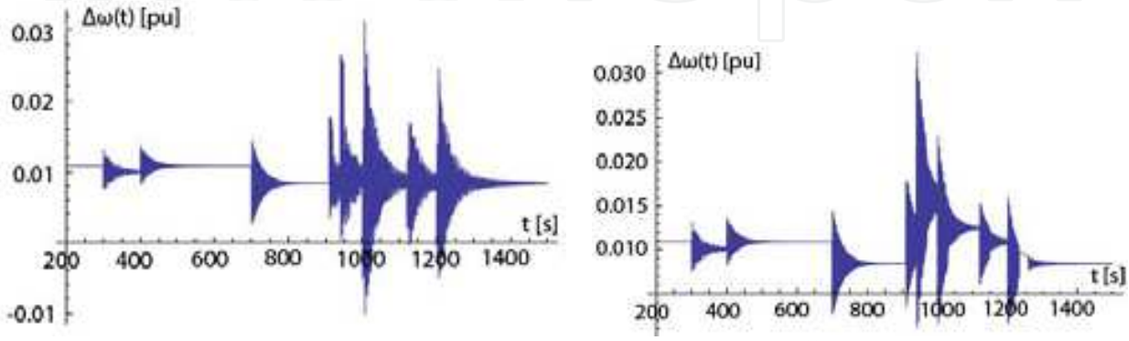

(e) (f)

Figs. 18e,f. (e) Transient response Δω(t) if only storage plant 4 absorbs the additional energy generated by WP plant with delay; (f) Transient response Δω(t) if none of the storage plants absorbs a substantial amount of energy generated by WP plant

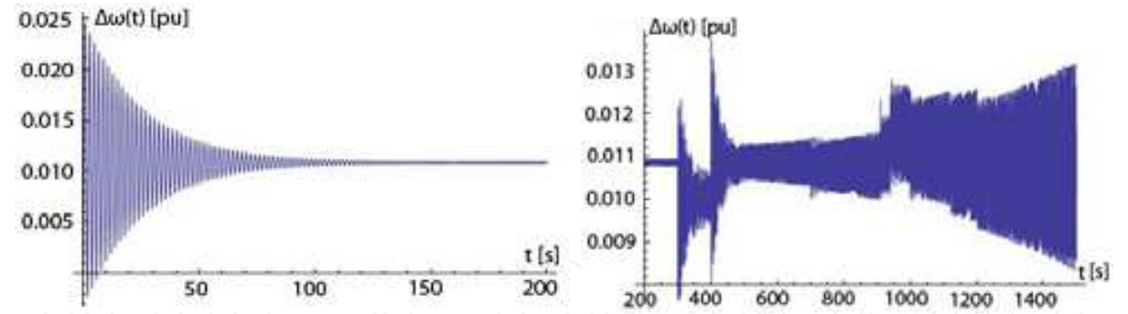

(a) (b)

Figs. 19a,b. (a) Steady-state stability is impaired as can be noticed in Fig. 19a at 200s and in Fig. 19b at 200 s; (b) Dynamic stability is lost after some load/demand changes have occurred

7. Power quality issues (steady-state and transient phenomena)

In addition to power balance issues, distributed renewable sources lead to high system impedance at the distribution level because these plants cannot deliver additional transient currents when faults occur due to their operation at peak power (Masoum *et al.*, 2002; Masoum *et al.*, 2004a). Even with acceptable current harmonics, this high system impedance may result in unacceptably high voltage harmonics, single-time events (e.g., spikes due to

network switching and synchronization) and non-periodic but repetitive (e.g., flicker) events, and contribute to power quality problems (E.F. Fuchs & Masoum, 2008a; E.F. Fuchs *et al.*, 2004; Masoum *et al.*, 2004b; E.F. Fuchs & Masoum, 2008b; Masoum *et al.*, 2004c; Masoum *et al.*, 2004d; E.F. Fuchs & H.A. Fuchs, 2008).

8. Conclusions

A review of existing frequency control practices based on droop characteristics and PSpice analyses of PWM rectifiers and inverters make clear that these components are ideal in a mix of short-term and long-term storage power plants. The complementary control algorithm as outlined in Figs. 17a,b,c and illustrated in Figs. 18, 19 permits intermittently-operating renewable sources to be matched with short-term and long-term storage plants so that the grid can be operated within a permissible frequency band of 59-61 Hz. However, if the intermittently operating plants are inactive for a longer time and the storage plants are depleted, demand-side management (e.g., load shedding) must be relied on.

In particular, the stability of a smart/microgrid consisting of natural gas-fired power plant (frequency leader), a long-term storage power plant and two intermittently operating plants (e.g., PV and WP plants) with associated short-term storage plants is assured if the following constraints are satisfied:

1. frequency variation is minimized through appropriate switching in and out of short-term storage plants;
2. transmission line parameters are optimized;
3. time constants of governors and valves are within feasible regions; and
4. droop characteristics of the individual plants must satisfy certain constraints.

9. References

Fuchs, E.F.; Masoum, M.A.S. (2008a). *Power Quality in Power Systems and Electrical Machines*, Elsevier/Academic Press, ISBN: 978-0-12-369536-9, Burlington, MA 01803, USA.

Fuchs, E. F.; Fuchs, H. A. (2007). Distributed Generation and Frequency/Load Control of Power Systems, *Proceedings of the 40th Annual Frontiers of Power Conference*, Oklahoma State University, Stillwater, Oklahoma, Oct. 29-30, 2007, pp. II-1 to II-9.

Fuchs E.F.; Fuchs, F.S. (2008). Intentional Islanding – Maintaining Power Systems Operation During Major Emergencies, *Proceedings of the 10th IASTED International Conference on Power and Energy Systems (PES 2008)*, ISBN: 978-0-88986-738-3, Baltimore, Maryland, pp. 156-162.

Wood, A. J.; Wollenberg, B. F. (1984). *Power Generation Operation & Control*, John Wiley & Sons, Inc., ISBN 13: 9780471586999.

Fuller, J. F.; Fuchs, E. F.; Roesler, D. J. (1989). Influence of Harmonics on Power System Distribution Protection, *IEEE Trans. on Power Delivery*, April 1988, Vol. TPWRD-3, No. 2, pp. 546- 554.

Fuchs E. F.; Masoum, M. A. S. (2011). *Power Conversion of Renewable Energy Systems*, Springer-Verlag, New York, ISBN: 978-1-4419-7978-0.

Defree, S. (2009). http://www.edn.com/article/459288-Photovoltaic_market_to_see_17_growth_rate_Gartner_reports.php, 1 page.

NREL (2009). Data from NREL's "Sun Spot One" Data Collection Station in the Colorado San LuisValley, available from http://www.nrel.gov/midc/ss1/

Masoum, M. A. S.; Dehbonei, H.; Fuchs, E. F. (2002). Theoretical and Experimental Analyses of Photovoltaic Systems with Voltage-and Current-Based Maximum Power Point Tracking, *IEEE Trans. on Energy Conversion*, Vol. 17, No. 4, (Dec. 2002), pp. 514-522.

Masoum, M. A. S.; Mousavi Badejani, S. M.; Fuchs, E. F. (2004a). MicroProcessor-Controlled New Class of Optimal Battery Chargers for Photovoltaic Applications, *IEEE Trans. on Energy Conversion*, Vol. 19, No. 3, Sept. 2004, pp. 599-606.

IEEE Standard 519 (1992). IEEE Recommended Practices and Requirements for Harmonic Control in Electric Power Systems, IEEE-519, 1992.

IEC 61000-3-2 (2001-10). Consolidated Edition, Electromagnetic Compatibility (EMC) – Part 3-2: Limits for Harmonic Current Emissions.

Yildirim, D.; Fuchs, E. F.; Batan, T. (1998). Test Results of a 20 kW, Direct-Drive, Variable-Speed Wind Power Plant, *Proceedings of the International Conference on Electrical Machines, Istanbul*, Turkey, Sept. 2-4, 1998, pp. 2039-2044.

Fuchs, E. F.; Myat, M. H. (2010). Speed and Torque Range Increases of Electric Drives Through Compensation of Flux Weakening, *Proceedings of the 20th International Symposium on Power Electronics, Electrical Drives, Automation, and Motion*, Pisa, Italy, June 14 - 16, 2010,pp. 1569-1574.

Cowdrey, J. (2004). Boulder's Municipal Hydroelectric System, July 7, 2004, 16 pages.

Mattick, W.; Haddenhorst, H. G.; Weber, O.; Stys, Z.S. (1975). Huntorf- the World's First 290 MW Gas Turbine Air Storage Peaking Plant, *Proceedings of the American Power Conference*, Vol. 37, 1975, pp. 322-330.

Vosburgh, K. G. (1978). Compressed Air Energy Storage, *J Energy*, Vol. 2, No. 2, March-April 1978, pp. 106-112.

Glems (1964). http://www.enbw.com/content/de/der_konzern/_media/pdf/imagebroschuere_standorte/Pumpspeicherwerk_Glems.pdf , 4 pages

Raccoon Mountain (1975). http://www.tva.gov/sites/raccoonmt.htm

Fuchs, E. F.; Roesler, D. J.; Masoum, M. A. S. (2004). Are Harmonic Recommendations According to IEEE and IEC Too Restrictive?, *IEEE Trans. on Power Delivery*, Vol. 19, No. 4, Oct. 2004, pp. 1775-1786.

Masoum, M. A. S.; Ladjevardi, M.; Jafarian, A.; Fuchs, E. F. (2004b). Optimal Placement, Replacement and Sizing of Capacitor Banks in Distorted Distribution Networks by Genetic Algorithms, *IEEE Trans. on Power Delivery*, Vol. 19, No. 4 , Oct. 2004, pp. 1794-1801.

Fuchs, E. F.; Masoum, M. A. S. (2008b). Torques in Induction Machines Due to Low-Frequency Voltage/Current Harmonics, *International Journal of Power and Energy Systems*, Vol. 28, Issue 2, 2008, pp. 212- 221.

Masoum, M. A. S.; Jafarian, A.; Ladjevardi, M.; Fuchs, E. F.; Grady, W. M. (2004c). Fuzzy Approach for Optimal Placement and Sizing of Capacitor Banks in the Presence of Harmonics, *IEEE Trans. on Power Delivery*,Vol. 19, No. 2, April 2004, pp. 822-829.

Masoum, M. A. S.; Ladjevardi, M.; Jafarian, A.; Fuchs, E. F. (2004d). Optimal Placement, Replacement and Sizing of Capacitor Banks in Distorted Distribution Networks by Genetic Algorithms, *IEEE Trans. on Power Delivery*, Vol. 19, No. 4, Oct. 2004, pp. 1794-1801.

Fuchs, E. F.; Fuchs, H. A. (2008). Power Quality of Electric Machines and Power Systems, *Proceedings of the 8thIASTED International Conference on Power and Energy Systems (EuroPES 2008)*, June 16–18, 2008, Corfu, Greece, paper # 608-035, 9 pages.

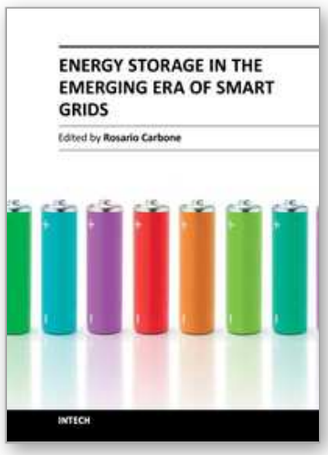

Energy Storage in the Emerging Era of Smart Grids

Edited by Prof. Rosario Carbone

ISBN 978-953-307-269-2
Hard cover, 478 pages
Publisher InTech
Published online 22, September, 2011
Published in print edition September, 2011

Reliable, high-efficient and cost-effective energy storage systems can undoubtedly play a crucial role for a large-scale integration on power systems of the emerging â€œdistributed generationâ€ (DG) and for enabling the starting and the consolidation of the new era of so called smart-grids. A non exhaustive list of benefits of the energy storage properly located on modern power systems with DG could be as follows: it can increase voltage control, frequency control and stability of power systems, it can reduce outages, it can allow the reduction of spinning reserves to meet peak power demands, it can reduce congestion on the transmission and distributions grids, it can release the stored energy when energy is most needed and expensive, it can improve power quality or service reliability for customers with high value processes or critical operations and so on. The main goal of the book is to give a date overview on: (I) basic and well proven energy storage systems, (II) recent advances on technologies for improving the effectiveness of energy storage devices, (III) practical applications of energy storage, in the emerging era of smart grids.

How to reference

In order to correctly reference this scholarly work, feel free to copy and paste the following:

E. F. Fuchs and W. L. Fuchs (2011). Complementary Control of Intermittently Operating Renewable Sources with Short- and Long-Term Storage Plants, Energy Storage in the Emerging Era of Smart Grids, Prof. Rosario Carbone (Ed.), ISBN: 978-953-307-269-2, InTech, Available from: http://www.intechopen.com/books/energy-storage-in-the-emerging-era-of-smart-grids/complementary-control-of-intermittently-operating-renewable-sources-with-short-and-long-term-storage

INTECH
open science | open minds

InTech Europe
University Campus STeP Ri
Slavka Krautzeka 83/A
51000 Rijeka, Croatia
Phone: +385 (51) 770 447
Fax: +385 (51) 686 166
www.intechopen.com

InTech China
Unit 405, Office Block, Hotel Equatorial Shanghai
No.65, Yan An Road (West), Shanghai, 200040, China
中国上海市延安西路65号上海国际贵都大饭店办公楼405单元
Phone: +86-21-62489820
Fax: +86-21-62489821

IntechOpen